Reactive nitrogen species (RNS) and its reaction intermediates with reactive oxygen species (ROS) in pH-neutral high-strength plasma-activated water determines the antimicrobial activity against ESKAPE Pathogens

Debapriya Mukherjee[1#], Atish Roy Chowdhury[1#], Pallab Ghosh[1#], Nishanth Vishwa[2], Lakshminarayana Rao[*2], Dipshikha Chakravortty[*1,3]

1 Department of Microbiology and Cell Biology, Indian Institute of Science, Bangalore, India

2 Centre for Sustainable Technologies, Indian Institute of Science, Bangalore, India

2 Interdisciplinary Centre for Water Research, Indian Institute of Science, Bangalore, India

3 School of Biology, Indian Institute of Science Education and Research, Thiruvananthapuram, India

 # Equal contribution

*** Corresponding Authors**

Lakshminarayana Rao, Centre for Sustainable Technologies, Indian Institute of Science, Bangalore, Karnataka 560012, India.

Email: narayana@iisc.ac.in

Dipshikha Chakravortty, Department of Microbiology and Cell Biology, Indian Institute of Science, Bangalore, Karnataka 560012, India.

Email: dipa@iisc.ac.in

Abstract

Plasma activated water (PAW) has gained significant global recognition due to its diverse applications in the biomedical and food preservation industries. The interaction between plasma's ionized particles, comprising ions, electrons, and neutral atoms, and water molecules results in high concentrations of reactive oxygen species (ROS) and reactive nitrogen species (RNS), making PAW effective across various medical and agricultural fields. Previous research has demonstrated that effectiveness of PAW largely depends on its acidic pH, which generates several nucleophilic oxidants or secondary reactive nitrogen intermediates, such as peroxynitrite, derived from primary ROS and RNS. In one of our earlier studies, we were successful in generation of PAW at a neutral pH, which is more practical for real world applications. In this research, we explored the potential of the neutral pH high strength buffered PAW (hsPAbW) as an antimicrobial agent against ESKAPE pathogens and investigated its mechanism of action. Our findings revealed that hsPAbW effectively reduced bacterial viability during their exponential growth phase. We demonstrated that the ROS in hsPAbW are insufficient to independently kill the bacteria. Instead, the RNS components of hs-PAbW can exert microbicidal effects either independently or through the formation of peroxynitrite intermediates, which lead to nitrotyrosine production. As a result, we eliminated the need for low pH to induce the antimicrobial effects of hsPAbW, making it more practical for real world applications. Finally, our study showed that hs-PAbW is more effective at killing bacteria than high doses (50 microgram/mL) of antibiotics like ceftazidime, ciprofloxacin, and meropenem. Overall, our research highlights the promising potential of neutral pH PAW as a sustainable solution for combating ESKAPE pathogens.

Keywords: Plasma-activated water (hs-PAbW), reactive oxygen species (ROS), reactive nitrogen species (RNS), peroxynitrite, ESKAPE pathogens, enteropathogen, antibiotics.

Introduction

World Health Organization has recognized antimicrobial resistance (AMR) as one of the severe threats to global health in the current century [1, 2]. Bacteria can achieve AMR in two different ways, one is 'intrinsic,' where the bacteria can build resistance against a class of antibiotics by inducing mutations in its genome, and the other is 'acquired,' which is attained by mobile genetic elements [3]. According to the reports published by US Centre for Disease Control and Prevention (CDC), every year, more than two million individuals are infected with antibiotic-resistant infections in the US, resulting in at least 23000 deaths [1]. In 2019, 1.27 million deaths were reported worldwide due to bacterial antimicrobial resistance [4]. *Acinetobacter baumannii*, *Pseudomonas aeruginosa,* and non-typhoidal *Salmonella* are a few of the bacterial pathogens which are predominantly associated with AMR-related deaths [1, 4]. This is why developing a novel, long-lasting, and sustainable solution for bacterial infections remains a significant challenge.

Plasma-activated water (PAW) is an emerging technology that has gained attention for its potential as a sustainable solution to various medical and food preservation applications [5-7]. PAW is produced by exposing water to cold plasma, an ionized gas containing charged particles like ions, electrons, and neutral atoms [8]. The ionized particles in the plasma interact with the water molecules generating reactive oxygen species (ROS) and reactive nitrogen species (RNS) [9]. These ROS and RNS generated have varying lifetimes, ranging from a few nanoseconds to a few years [10, 11]. Various applications of PAW such as anti-cancer [7], antimicrobial [12], anti-viral [13], food preservation [5, 14], insecticidal [15], oral hygiene [16, 17] and anti-fungal [18] have been demonstrated by various researchers. These studies have mostly worked with acidic pH PAW [10, 18, 19]. Real-world application of PAW requires the generation of neutral

pH PAW, which has been successfully designed by our group before [20, 21]. This study presents a translational application of neutral pH PAW (hs-PAbW) against ESKAPE pathogens. ESKAPE pathogens can cause a wide array of infections that include hospital-acquired nosocomial infections and pneumonia, surgical site infections, wound infections, and infections of the blood and urinary tract [22, 23]. In the current study, we have demonstrated the bactericidal potential of the neutral-pH hs-PAbW (pH range- 7 to 7.4) and investigated the mechanism of kill on four ESKAPE pathogens, namely *Staphylococcus aureus*, hyper viscous *Klebsiella pneumoniae*, *Acinetobacter baumannii*, and *Pseudomonas aeruginosa*. We found that hs-PAbW could successfully reduce the viability of all four bacterial strains during their exponential growth phase. Interestingly, when we generated hs-PAbW containing only one of the functional components, ROS (in the same levels as hs-PAbW) in ROS-PAW (H_2O_2), it lost its bactericidal activity. However, RNS-PAbW, with functional components (NO_2^-, NO_3^-) at similar concentrations as hs-PAbW, successfully reduced the bacterial load. We also demonstrated that RNS in both RNS-PAbW and hs-PAbW generates peroxynitrite, which leads to the formation of nitrotyrosine residues, ultimately causing the bactericidal effect, independent of acidic pH. Furthermore, our study revealed that hs-PAbW is more effective at killing bacteria than high doses (50 µg/mL) of ceftazidime, ciprofloxacin, and meropenem.

Results

Neutral pH plasma-activated water could kill the bacteria from the exponential growth phase.

The hs-PAbW consists of NO_2^-, NO_3^-, and H_2O_2 (for the current study, NO_2^- 600 mg/ L, NO_3^- 130 mg/ L, and H_2O_2 200 mg/ L) [19]. The adverse effect of intracellular reactive nitrogen and reactive oxygen species (RONS) on the growth of tissue-invading pathogens has been well studied [24, 25]. The free radicals generated in *in-vitro* H_2O_2, and acidified nitrite can also

efficiently kill a wide range of amoebal, fungal, and bacterial pathogens [26, 27]. PAW is considered as a green alternative technology in biomedicine and can inhibit the growth of human breast cancer cells (MDA-MB-231) at a pH of around 1.9 [28]. In one of our previous studies, we have shown a strategy to generate a hs-PAbW within a pH range of 7 to 7.4 [21]. We have also tested the antimicrobial effect of neutral-pH hs-PAbW on the enteropathogen *Salmonella* Typhimurium [20]. However, the effect of hs-PAbW, with neutral pH, on the growth of virulent ESKAPE pathogens remains to be investigated. ESKAPE pathogens have emerged as MDR and XDR strains against all traditional antimicrobials and are associated with acute and chronic respiratory and gastrointestinal illnesses. To assess the role of hs-PAbW in inhibiting the growth of ESKAPE pathogens, we subjected *Staphylococcus aureus*, hyper viscous *Klebsiella pneumoniae*, *Acinetobacter baumannii*, and *Pseudomonas aeruginosa* to the hs-PAbW treatment for 45 minutes. To ascertain the role of hs-PAbW on the specific growth phase of bacteria, we incubated both exponential and stationary phase cultures of bacteria with hs-PAbW. DAF_2DA staining of hs-PAbW-treated log phase cultures of *Staphylococcus* **(Figure S1A and S1B)**, *Klebsiella* **(Figure S1C and S1D)**, *Acinetobacter* **(Figure S1E and S1F)**, and *Pseudomonas* **(Figure S1G and S1H)** showed significantly higher amounts of RNS compared to the control water treatment (*Staphylococcus*- hs-PAbW-28.89%, control-1.33%, *Klebsiella* - hs-PAbW-47.02%, control-5.9%, *Acinetobacter*- hs-PAbW-62.18%, control-8.3%, and *Pseudomonas*- hs-PAbW-63.7%, control-32.73%). A similar trend was observed when the stationary phase cultures of the bacteria were treated with hs-PAbW **(Figure S2A- S2H)**. Similarly, stationary phase *Staphylococcus* **(Figure S2A and S2B)**, *Klebsiella* **(Figure S2C and S2D)**, *Acinetobacter* **(Figure S2E and S2F),** and *Pseudomonas* **(Figure S2G and S2H)** treated with hs-PAbW generated higher amounts of RNS (*Staphylococcus*-43.72%, *Klebsiella*-80.77% *Acinetobacter*-59.12%, and *Pseudomonas*- 95.37%) compared to the control-treated set (*Staphylococcus*-2.15%, *Klebsiella*- 13.69% *Acinetobacter*-11.6%, and *Pseudomonas*-

37.25%). We hypothesized that a high level of RNS present in hs-PAbW would significantly reduce bacterial viability. To show hs-PAbW-dependent killing of the bacteria, hs-PAbW-treated log **(Figure 1)** and stationary phase **(Figure S3)** cultures of *Staphylococcus*, *Klebsiella*, *Acinetobacter*, and *Pseudomonas* were subjected to PI staining. The higher PI-positive percent population of *Staphylococcus* (hs-PAbW-18.09%, control-4.02%), *Klebsiella* (hs-PAbW-30.86%, control-4.02%), *Acinetobacter* (hs-PAbW-10.34%, control-2.64%), and *Pseudomonas* (hs-PAbW-8.62%, control-3.57%) suggested a drastic reduction in the survival of log phase bacteria under hs-PAbW treatment **(Figure 1A- 1H)**. This was consistent with the observations for PI staining in *Salmonella* was in line with our previous data [20]. On the contrary, we found no difference in the bacterial viability when stationary phase cultures of *Staphylococcus* (hs-PAbW-3.49%, control-2.83%), *Klebsiella* (hs-PAbW-11.99%, control-9.64%), *Acinetobacter* (hs-PAbW-4.48%, control-4.41%), and *Pseudomonas* (hs-PAbW-1.57%, control-2.67%) were treated with hs-PAbW **(Figure S3A-S3H)**.

The oxygen (H_2O_2) and nitrogen (NO_2^-, NO_3^-) species present in hs-PAbW independently cannot kill bacterial pathogens.

As discussed earlier, hs-PAbW consists of both oxygen (H_2O_2) and nitrogen (NO_2^- and NO_3^-) species. The microbicidal activity of hs-PAbW can be attributed to its high content of ROS and RNS. We sought to identify the role of each of these functional components in reducing bacterial growth. As we found that hs-PAbW can restrict bacterial growth at the exponential phase, we subjected the log phase cultures of all three bacterial strains to the treatment with ROS-PAW **(Figure 2)** and RNS-PAbW **(Figure 3)**. The higher percent population and median fluorescence intensity (MFI) of DCFDA for the ROS-PAW treated bacterial samples suggested the generation of high concentrations of ROS **(Figure S4)**. Treating the *Staphylococcus*, *Klebsiella*, *Acinetobacter*, and *Pseudomonas* with ROS-PAW gave rise to 56.88%, 27.12%, 63.57%, and 85.73% of DCFDA-positive population compared to the control water

(*Staphylococcus*-7.34%, *Klebsiella*-1.36%, *Acinetobacter*-52.17%, and *Pseudomonas*-60.29%) **(Figure S4A-S4E)**. The higher MFI value for DCFDA in ROS-PAW treated samples further supported this observation **(Figure S4F)**. When the level of bacterial death by ROS-PAW treatment was determined by PI staining, we observed that, unlike hs-PAbW, it was inefficient to kill bacteria despite high intracellular ROS levels **(Figure 2)**. This was established by the comparable PI-positive percent population of *Staphylococcus* (ROS-PAW-2.54% and control water-1.26%), *Klebsiella* (ROS-PAW-5.54% and control water- 5.36%) *Acinetobacter* (ROS-PAW-1.82%, control water-2.38%), and *Pseudomonas* (ROS-PAW-0.44%, control water-1.73%) between ROS-PAW and control water treatments **(Figure 2A-2E)**. In line with this observation, a comparable MFI value was observed between ROS-PAW and control water-treated bacterial samples **(Figure 2F)**. The greater DAF_2DA-positive percent population **(Figure S5A-S5E)** and higher relative MFI value **(Figure S5F)** corresponding to RNS-PAbW-treated bacterial cells (*Staphylococcus*; RNS-PAbW-33.41%, control water-3.97%, *Klebsiella*; RNS-PAbW-54.9%, control water-2.09%, *Acinetobacter*; RNS-PAbW-30.41%, control water-7.17%, and *Pseudomonas*; RNS-PAbW-75.08%, control water-23.18%) further showed that treating the bacterial cells with RNS-PAbW generated high concentration of reactive nitrogen species **(Figure S5A-S5E)**. Surprisingly, when we quantified the level of reduction in bacterial viability by RNS-PAbW treatment, we observed that unlike ROS-PAW, RNS-PAbW could kill the actively growing *Staphylococcus* (RNS-PAbW-95.99% and control water-1.68%), *hv Klebsiella* (RNS-PAbW-44.62% and control water-4.18%), *Acinetobacter* (RNS-PAbW-88.34%, control water-5.83%), and *Pseudomonas* (RNS-PAbW-51.03%, control water-3.8%) **(Figure 3A-3E)**. Compared to the control water-treated cells, the increased relative MFI of PI for RNS-PAbW-treated bacteria further corroborated our observation **(Figure 3F)**. The reduction in Colony Forming Units (CFU) after exposure to RNS-PAbW and hs-PAbW, but not ROS-PAW, further confirmed the results obtained from PI staining **(Figure S6)**. Taken together,

we could conclude that RNS is the major factor contributing to the microbicidal activity of hs-PAbW (pH=7 to 7.4) in ESKAPE pathogens.

High concentration of peroxynitrite in RNS-PAbW and hs-PAbW is one of the factors regulating the microbicidal role of hs-PAbW.

We visualized the damage caused by hs-PAbW on the ESKAPE pathogens under Scanning Electron Microscopy (SEM) **(Figure 4A)**. Morphological changes were observed in hv *Klebsiella*, *Acinetobacter*, and *Pseudomonas* following treatment with hs-PAbW compared to the control water treatment. hv *Klebsiella* exhibited shrunken, distorted structures and clumping after hs-PAbW exposure. Untreated *A. baumannii* maintained smooth surface morphologies, while exposure to hs-PAbW caused visible distortions, indicating cellular lysis. *P. aeruginosa* exhibited reduction in cell size and clumping post treatment. Exposure to ROS-PAW and RNS-PAbW led to noticeable alterations in surface morphology across all three bacterial strains, including changes in cell size, as seen through SEM. **(Figure S7)**. Overall, no noticeable morphological changes were observed in the Gram-positive bacterium *S. aureus* after treatment with any of the water samples. Previous studies on *Fusarium graminearum* spores have indicated that PAW can reduce cell membrane potential and compromise membrane integrity. In the same study, they attributed the significant increase in the leakage ratio of DNA/RNA and proteins to intracellular content leakage, resulting from cell membrane damage caused by PAW treatment [29]. This piqued our interest in determining whether a similar process occurred with our water samples. To investigate this, we employed the membrane-potential sensitive dye $DiBAC_4$ following incubation with the respective water samples. PAW can damage the cell wall and membrane by oxidizing unsaturated fatty acids in the lipid bilayer, breaking peptide bonds, and oxidizing amino acid side chains [30]. Our results

showed that *P. aeruginosa*, hv *K. pneumoniae*, and *A. baumannii* exhibited higher relative MFI after exposure to the test water samples, indicating greater membrane depolarization **(Figure 4C-E)**. In contrast, *S. aureus* displayed lower relative MFI, suggestive of membrane hyperpolarization **(Figure 4B)**. In conclusion, we found that both ROS-PAW and RNS-PAbW could exhibit the ability to alter membrane potential; however, the former was unable to produce a bactericidal effect despite this. Therefore, the alteration of membrane potential may not be the factor responsible for the bactericidal effect of hs-PAbW.

Following this, we wanted to further characterize the predominant chemical species contributing to the bactericidal activity of the neutral pH PAW. To achieve this, it is crucial to understand the differences in composition and how the varying components function. Our previous data had shown a significant increase in the Propidium-Iodide positive population upon treatment with the RNS-PAbW. Since the RNS-PAbW was enriched in NO_2^- and NO_3^- in the range of hs-PAbW, we can conclude that the RNS in hs-PAbW were conferring the microbicidal activity of hs-PAbW against ESKAPE pathogens tested. Apart from ROS and RNS, hs-PAbW is also comprised of short-lived species like peroxynitrous acid (ONOOH) and peroxynitrite ($ONOO^-$) [6, 8, 20]. Peroxynitrite can lead to cell damage by direct oxidation of target molecules or by indirect effects mediated by its decomposition products [31]. In order to delineate the involvement of short-lived species like peroxynitrite in the bactericidal role of hs-PAbW, we first proceeded to do an intracellular peroxynitrite estimation following individual treatments **(Figure 4F-4I)**. We found that there was no significant change in the peroxynitrite levels between control ROS water and ROS-PAW. However, there was a significant increase in the peroxynitrite levels upon treatment with RNS-PAbW and hs-PAbW compared to their control counterparts. In *Staphylococcus* and hv *Klebsiella* logarithmic phase cultures we found that RNS-PAbW produced a significantly higher concentration of peroxynitrite as compared to hs-PAbW **(Figure 4F-G)**. In *Acinetobacter* and *Pseudomonas* cultures, there was no significant

change in the concentration of peroxynitrite produced by RNS-PAbW and hs-PAbW **(Figure 4H-I)**. This shows that RNS present in the hs-PAbW leads to the formation of peroxynitrite radicals in the latter.

Treatment with RNS-PAbW, hs-PAbW, and ROS-PAbW caused a reduction in the length, height, and Young's modulus of the Gram-negative bacterium hv *Klebsiella pneumoniae* although ROS-PAW was unrelated to increased nitrotyrosine levels in *S. aureus* and *K. pneumoniae*

To further investigate the antimicrobial mechanisms of neutral pH high-strength hs-PAbW, we selected *Staphylococcus aureus* and hv *Klebsiella pneumoniae* as representative Gram-positive and Gram-negative bacteria, respectively. To quantify the morphological changes in the two bacterial species after treatment, logarithmic phase cultures of both were exposed to different water samples, and their morphological characteristics were evaluated using Atomic Force Microscopy **(Figure 5A-G)**. In line with our SEM data, the results showed that treatment with the water samples did not induce any significant changes in the length, height, or Young's modulus of the Gram-positive bacterium, *Staphylococcus aureus* **(Figure 5B-D)**. In contrast, exposure of hv *Klebsiella pneumoniae* to RNS-PAbW, hs-PAbW, and ROS-PAbW resulted in a significant reduction in the length, height, and Young's modulus **(Figure 5E-G).** This further supports our earlier idea that, while ROS-PAW may not be effective in killing bacteria, it can still affect their structural integrity. This supports the notion that reactive nitrogen species (RNS) and short-lived species like peroxynitrite, rather than reactive oxygen species (ROS), are responsible for the bactericidal effects of hs-PAbW.

Peroxynitrous acid has the ability to nitrate both free and protein-bound tyrosine [32]. Tyrosine nitration at the 3-position is recognized as a biomarker for peroxynitrite formation *in vivo* [33].

When protein-bound tyrosine is nitrated, it may disrupt the protein's structure and function [34]. During phagocytosis, macrophages produce peroxynitrite, leading to the oxidation and nitration of proteins within the engulfed pathogen. This process serves as a key defence mechanism against invading pathogens.[35]. In our study, nitrotyrosine estimation indeed revealed a significant presence of the residue in the cell lysates of both Gram-positive *Staphylococcus aureus* and Gram-negative hv *Klebsiella pneumoniae* following exposure to hs-PAbW and RNS-PAbW **(Figure 5H)**. This suggests that peroxynitrite is actively formed in these bacteria, contributing to the antimicrobial effects observed. As expected, nitrotyrosine levels were undetectable in bacteria treated with control water and ROS-PAW, further supporting the conclusion that RNS and peroxynitrite plays a critical role in the bactericidal activity of neutral pH hs-PAbW. The standard curve and raw data for nitrotyrosine quantification are provided in supplementary data **(Figure S8)**.

Compared to high concentrations of antibiotics, hs-PAbW showed more efficiency in killing ESKAPE and enteropathogen.

Both ceftazidime (a third-generation cephalosporin) and meropenem (a carbapenem) are β-lactam antibiotics. They are routinely used in treating a wide range of bacterial infections, including MDR and ESBL *Enterobacterales*, *Pseudomonas aeruginosa*, and *Klebsiella pneumoniae* [36-38]. Ciprofloxacin belongs to the category of fluoroquinolone and inhibits the growth of several pathogens, such as *Acinetobacter sp.* and *Salmonella sp,* by blocking the activity of DNA gyrase (*gyrAB*) [39, 40]. As we observed that hs-PAbW could successfully reduce the viability of actively growing bacteria, we decided to compare its bactericidal activity with these antibiotics. We harvested bacteria from the log phase of their growth and subjected them to the treatment of either high concentrations of antibiotics (ceftazidime, ciprofloxacin, and meropenem, concentration- 50 µg/ mL) or hs-PAbW for 45 minutes. Surprisingly, we observed that hs-PAbW is more efficient than ceftazidime, ciprofloxacin, and meropenem in

inducing bacterial death **(Figure 6)**. Forty-five minutes of treatment with hs-PAbW caused significantly higher death in all three bacterial strains (*Staphylococcus*- hs-PAbW-5.52%, *Klebsiella*- 16.65%, *Acinetobacter*-27.09%, and *Pseudomonas*-15.42%) compared to the antibiotics treatment (*Staphylococcus*- ceftazidime-1.9%, ciprofloxacin-1.2%, meropenem 1.73%, *Klebsiella*- ceftazidime-5.04%, ciprofloxacin-1.85%, meropenem 2.04%, *Acinetobacter*- ceftazidime-1.33%, ciprofloxacin-1.54%, meropenem-1.43%, and *Pseudomonas*- ceftazidime-0.99%, ciprofloxacin-0.84%, meropenem-1.49%) **(Figure 6A-6F)**. Altogether, our study showed that hs-PAbW works faster than the high dose of antibiotics and induces death in actively growing pathogenic bacteria. To the best of our knowledge, this is the first study to propose RNS-mediated, neutral pH PAW as a therapeutic agent for translational applications.

Discussion

World Health Organization has recognized Surgical Site Infection (SSI) as the most surveyed Healthcare-Associated Infections (HAIs) in low and middle-income countries, which results in post-operative morbidity, mortality, prolonged hospital stays, and increased healthcare expenditures [41-43]. SSIs are correlated with the types of wounds and vary with the site of surgeries. These infections are majorly caused by either exogenous (from the environment of the operation theatre or the surgical ward) or endogenous (resident microbiota from the patient's skin or opened viscus) bacterial pathogens. The imbalances between the local pathological factors and immune defences in post-operative chronic wounds, due to the presence of cytolytic enzymes like matrix metalloproteinases (MMPs), free oxygen radicals, and inflammatory mediators [44, 45], promote the colonization of several pathogenic bacteria such as *Pseudomonas aeruginosa* and *Acinetobacter baumannii* [46-48]. During bacterial

infection, the rapid, excessive, and indiscriminate use of antibiotics gives rise to antimicrobial resistance (AMR) worldwide [49]. So discovering a novel and sustainable cure for wound-site bacterial infection is a significant challenge in biomedicine [50].

The PAW, consisting of several polyatomic ions such as NO_2^-, NO_3^-, and H_2O_2 (in the current study: NO_2^- 600 mg/ L, NO_3^- 130 mg/ L, and H_2O_2- 200 mg/ L) showed significant potential in disrupting bacterial biofilms [51, 52]. The combination of nitric oxide and superoxide ions in acidic pH gives rise to several secondary reactive nitrogen intermediates, such as peroxynitrite ($ONOO^-$, ONOOH), which can function as nucleophilic oxidants [53, 54]. Due to its high ROS and RNS content (RONS), PAW is widely used in food and agricultural industries for disinfecting fruits and raw vegetables [11, 55]. The peroxynitrite and hydroxyl radicals of PAW induce the expression of defence-related genes in tomato seedlings [56]. Multiple studies showed that PAW has a wide application in the field of cancer biology [57]. It can induce apoptosis in B16F10 cancer cell lines [58]. Applying PAW-18 (pH=1.9) caused significant death in the MDA-MB-231 human breast cancer cells [28]. Multiple studies showed that acidic pH stabilizes and intensifies the activity of reactive oxygen and nitrogen species [59, 60]. In one of our previous studies, we demonstrated that using bicarbonate water can effectively buffer and maintain the pH of PAW near neutrality (hs-PAbW), making it more practical for real-world applications. Additionally, we showed the antimicrobial effect of hs-PAbW on hv *Klebsiella pneumoniae* and methicillin-resistant *Staphylococcus aureus* (MRSA) in the same study [20]. However, the predominant chemical species that is bringing about the bactericidal role of hs-PAbW in absence of acidic pH remained to be understood.

In this study we have seen that DCF_2DA and DAF_2DA staining of hs-PAbW, ROS-PAW, and RNS-PAbW treated bacterial samples showed that the stability of RONS was equally maintained in the physiological pH range (between 7 and 7.4). However, when the cell viability was estimated, it was observed that hs-PAbW is more efficient in killing log-phase bacteria

than the stationary phase. The high rate of metabolic activity and basal respiration could be a reason for the greater sensitivity of the log phase culture of *Staphylococcus*, *Klebsiella*, *Acinetobacter*, and *Pseudomonas* to hs-PAbW [61]. Additionally, our study showed that ROS-PAW, which contained similar levels of ROS as hs-PAbW, couldn't kill the bacteria independently. This shows that the concentration of ROS present in ROS-PAW or hs-PAbW are unable to bring about the bactericidal effect. Instead, when they are incubated in RNS-PAbW where RNS are present at a specific proportion (as mentioned earlier), they execute the maximum bactericidal activity. Incubation in ROS-PAW and RNS-PAbW resulted in changes to the membrane potential of all the bacterial strains tested, similar to hs-PAbW. As reported previously, this effect may be caused by lipid peroxidation mediated by reactive species present in PAW, which leads to oxidative degradation of cholesterol, phospholipids, and unsaturated fatty acids, ultimately causing damage to the cell membrane [62-67]. Also, previous studies had shown that the thick cell wall in Gram-positive bacteria confers resistance to PAW. This explains why we observed no change in the size or stiffness of *S. aureus* upon exposure to any of the water samples [68].

Amongst the short-lived species, hs-PAbW exposure generated the peroxynitrite ion inside bacterial cells, which was also abundant in the RNS-PAbW-treated cells. Once at the bacterial membrane, peroxynitrite can enter the cell through passive diffusion (as peroxynitrous acid, ONOOH) or via anion channels (as the peroxynitrite anion, $ONOO^-$). Inside the cell, it can interact with various targets, leading to protein modifications [69], lipid oxidation [70], and DNA damage [71], either directly or indirectly through its decomposition products. Oxidative stress induced by peroxynitrite can result from the direct oxidation reactions of peroxynitrous acid or from the generation of oxidizing radicals (e.g., •OH). This can lead to the oxidation of lipids, thiols, and heme proteins, hydroxylation of aromatic rings, and damage to iron-sulphur clusters [72]. Nitrosative stress may occur due to the nitration of phenols and the nitrosylation

of thiols [69]. Peroxynitrite has also been shown to interact with and modify the function and/or stability of eukaryotic proteins such as lysozyme and phosphatase [73-75]. Abundance of intracellular peroxynitrite led to nitration at the 3-position of tyrosine, that can effectively interfere with the functionality of the bacterial proteins [34]. Due to negligible peroxynitrite formation upon ROS-PAW treatment, nitrotyrosine levels were also low in that condition. From this, we can conclude that nitrotyrosine formation is one of the primary mechanisms responsible for the bactericidal action of our neutral pH high-strength PAW. Our study also demonstrates that RNS in hs-PAbW is the key factor driving its bactericidal effect. As a result, we have successfully eliminated the need for acidic pH for PAW activity and developed neutral pH high-strength hs-PAbW, where the antimicrobial effect is mainly driven by RNS or short-lived species like peroxynitrite, whose production is also exclusively mediated by RNS.

Apart from their specific mode of action, antibiotics also generate a massive amount of ROS while effectively affecting the bacteria [38, 76, 77]. Ceftazidime, ciprofloxacin, and meropenem are potent antibiotics to treat several bacterial infections, including *Pseudomonas* and *Acinetobacter* [78-81]. To quantify the bactericidal activity of hs-PAbW, we treated the log-phase culture of the bacteria with hs-PAbW and high concentrations (50 µg/ mL) of these antibiotics for 45 minutes. A significant increase in the PI-positive population of *Staphylococcus*, hv *Klebsiella*, *Pseudomonas*, and *Acinetobacter*, compared to the antibiotic treated sets, showed that hs-PAbW could be used as an alternative antimicrobial therapy. It will be lucrative to use RNS mediated bactericidal role of hs-PAbW to counteract the AMR developing worldwide.

Materials and Methods

Bacterial strains and sample preparation

Staphylococcus aureus, hyper viscous *Klebsiella pneumoniae* (pus isolate 529) [21], *Acinetobacter baumannii* strain S2 (ATCC), and *Pseudomonas aeruginosa* PAO1 (a generous gift from Prof. Anne-Béatrice Blanc-Potard, Université de Montpellier) were revived on LB agar plates without antibiotics from glycerol stock stored at -80^0 C. One colony was inoculated in the LB broth and grown overnight in a shaking incubator (170 rpm) at 37^{0}C. At 12 hours post-infection, the stationary phase bacteria were subcultured into freshly prepared LB broth and incubated for 4 to 5 hours to obtain the exponential growth (log) phase. The $(OD)_{600}$ of the stationary and log phase bacterial cultures were adjusted to 0.3 (~10^8 CFU/ mL) and 0.1 (~10^6 CFU/ mL), respectively, and treated with either control or hs-PAbW, ROS-PAW, RNS-PAbW, and high concentration (50 µg/ mL) of antibiotics (ceftazidime, ciprofloxacin, and meropenem) for 45 minutes.

Generation of hs-PAbW, ROS-PAW, RNS-PAbW

We have generated hs-PAbW, ROS-PAW, RNS-PAbW by the protocol as described before. We have used the nomenclature hs-PAbW for our laboratory generated PAW and RNS-PAbW for our laboratory generated RNS rich PAW as we have used buffered water for both. Similar nomenclatures have been used in our previous study [20].

Flow cytometry analysis.

After treating the bacterial cells with either control water or hs-PAbW, ROS-PAW, RNS-PAbW, and antibiotics for 45 minutes, the cells were pelleted by centrifugation (6000 rpm for 10 minutes) and washed with double autoclaved milli-Q water. This was followed by the resuspension of bacterial cells in milli-Q water. Diaminofluorescein-2 diacetate (DAF_2DA) was added to the resuspended cells (final concentration- 10 µM) and incubated for 30 minutes to measure the level of reactive nitrogen species (excitation- 491 nm, emission- 513 nm) [82]. Similarly, the treated and resuspended bacterial cells were incubated with

dichlorodihydrofluorescein diacetate (DCFDA, final concentration- 10 µM, excitation- 492 nm, emission- 517 nm) [83], propidium iodide (PI, final concentration- 1 µg/ mL), bis-(1,3-dibutylbarbituric acid) (DiBAC4, final concentration-1 µg/ mL) [84] to estimate the level of reactive oxygen species and bacterial death, respectively. The samples were analysed by flow cytometry (BD FACSVerse from BD Biosciences-BS), and the data analysis was done with BD FACSuite software.

Bacterial spread plating

Logarithmic phase cultures of *Staphylococcus aureus*, hv *Klebsiella pneumoniae*, *Pseudomonas*, and *Acinetobacter* were centrifuged at 6,000 rpm for 10 minutes to pellet the cells. The pellets were resuspended in the water samples and incubated for 45 minutes. After incubation, the bacterial suspensions were serially diluted in 1X Phosphate Buffer Saline (PBS), and the appropriate dilutions were spread onto LB Agar plates. The plates were then incubated overnight at 37˚C under static conditions, and colony-forming units were noted.

Scanning Electron Microscopy

Logarithmic culture of *Staphylococcus*, hv *Klebsiella*, *Pseudomonas*, *Acinetobacter* were centrifuged at 6,000 rpm for 10 minutes. The supernatants were discarded, and the pellets were resuspended in the water samples. Post incubation of 45 mins, they were drop-casted on clear glass coverslips and air-dried. The samples were fixed by using 3.5% glutaraldehyde overnight at 4˚C. Next day, they were subjected to a serial dehydration step using 10, 30, 50, 70, 90, 100% alcohol. Following this, they were dried using a vacuum-desiccator. The samples were subjected to gold spluttering before imaging. Thermofischer XL-30 ESEM was used for the image acquisition.

Peroxynitrite Estimation Assay

The intracellular peroxynitrite assay was performed using Peroxynitrite Assay Kit from Abcam (ab2334690), using manufacturer's protocol. Briefly, the exponential phase cultures of the tested pathogens were incubated in control ROS water, ROS water, control (RNS-PAbW, hs-PAbW), RNS-PAbW, and hs-PAbW for 1 hour. Following this, the cells were centrifuged at 6,000 rpm for 10 minutes and the pellet was resuspended in fresh milliQ to exclude any chances of peroxynitrite contamination from the treatment waters. 50 µl of the cell suspension was incubated with 50 µl of the substrate for 20 minutes. Following this, the fluorescence intensities were measured using a Tecan microplate reader, with Ex/Em at 490/530 nm.

Atomic Force Microscopy

Atomic Force Microscopy was carried out following a modified version of the protocol outlined by Roy Chowdhury *et al* [38]. In summary, logarithmic phase cultures of *Staphylococcus aureus* and hv *Klebsiella pneumoniae* were centrifuged at 6,000 rpm for 10 minutes. The resulting pellets were then resuspended in 1 ml of each water sample. After 45 minutes of incubation, the bacterial suspensions were centrifuged again at 6,000 rpm for 10 minutes, and the pellets were fixed using 3.5% paraformaldehyde. A 50 µl aliquot of each diluted sample was drop-cast onto coverslips and allowed to air dry. The images were captured using the NX10 AFM, and the length, height, and Young's modulus of the bacterial cells were measured with XEI software.

Nitrotyrosine estimation

The logarithmic phase cultures of *Staphylococcus aureus* and hv *Klebsiella pneumoniae* were centrifuged at 6,000 rpm for 10 minutes. The resulting pellets were resuspended in 1 ml of each water sample. After 45 minutes of incubation, the resuspended bacterial cells were lysed via

sonication at 30% amplitude with 20-second pulses for a total of 4 minutes. Cell debris was removed by centrifugation at 13,000 rpm for 10 minutes at 4˚C. The cell lysate was then concentrated using a speed vac, and protein concentration was determined using the Bradford reagent. An equal amount of protein was used for nitrotyrosine estimation, following the manufacturer's instructions for the Nitrotyrosine ELISA Kit (ab210603) from Abcam.

Statistical Analysis

The number of biological and technical replicates used in each experiment have been reported in the figure legends. The statistical analyses were done by unpaired two-tailed student's t-test as indicated in the figure legends. The *p* values below 0.05 were considered significant. The results were expressed as mean ± SEM. GraphPad Prism 8.4.3 (686) was used to generate the bar graphs and perform the statistical tests.

Author contribution

Conceptualization: DM, ARC, LNR, and DC, Methodology: DM, ARC, PG, NV , Investigation: DM, ARC, PG, NV, Visualization: DM,ARC , Data curation: DM, ARC, PG, Formal analysis: DM, ARC, Fund acquisition: LNR and DC, Project administration: DM, ARC, LNR, and DC, Writing-original draft: DM, ARC, and LNR, Editing and proofreading: PG, and DC, Supervision: LNR and DC.

Acknowledgments

The authors thank the central flow cytometry facility at IISc. Mrs. Dharani and Mr. Munish from the central flow cytometry facility are acknowledged for their help in FACS data

acquisition. Mrs. Deepika from Advanced Facility for Microscopy and Microanalysis (AFMM), IISc is acknowledged for her help in acquiring Scanning Electron Microscopy (SEM) images. Mrs. Monisha from Atomic Force Microscopy (AFM) Facility, Department of Bioengineering (BE), IISc, is acknowledged for her help in acquiring the AFM images.

Funding

This work was financially supported by the DAE SRC fellowship (DAE00195) and the DBT-IISc partnership umbrella program for advanced research in biological sciences and Bioengineering. Technical support from ICMR (Centre for Advanced Study in Molecular Medicine), DST (FIST), and UGC (special assistance) is duly acknowledged. DC acknowledges the ASTRA Chair professorship grant from IISc and TATA innovation fellowship grant. ARC thanks the IISc fellowship from MHRD, Govt. of India, and the late Dr. Krishna S. Kaikini estate for the Shamrao M. Kaikini and Krishna S. Kaikini scholarship. DM and PG sincerely thanks for the IISc fellowship from MHRD, Govt. of India. The authors thank the IISc and DST‐SERB for the financial support through the research grant EMR/2017/001016.

Competing Interest

The authors declare there exists no competing interest between them.

Reference

1. Prestinaci, F., P. Pezzotti, and A. Pantosti, *Antimicrobial resistance: a global multifaceted phenomenon.* Pathog Glob Health, 2015. **109**(7): p. 309-18.
2. Larsson, D.G.J. and C.F. Flach, *Antibiotic resistance in the environment.* Nat Rev Microbiol, 2022. **20**(5): p. 257-269.
3. Darby, E.M., et al., *Molecular mechanisms of antibiotic resistance revisited.* Nat Rev Microbiol, 2023. **21**(5): p. 280-295.
4. Antimicrobial Resistance, C., *Global burden of bacterial antimicrobial resistance in 2019: a systematic analysis.* Lancet, 2022. **399**(10325): p. 629-655.
5. Rajan, A., et al., *Plasma processing: a sustainable technology in agri-food processing.* Sustainable Food Technology, 2023. **1**(1): p. 9-49.

6. Thirumdas, R., et al., *Plasma activated water (PAW): Chemistry, physico-chemical properties, applications in food and agriculture.* Trends in Food Science & Technology, 2018. **77**: p. 21-31.
7. Girard, P.M., et al., *Synergistic Effect of H2O2 and NO2 in Cell Death Induced by Cold Atmospheric He Plasma.* Sci Rep, 2016. **6**: p. 29098.
8. Hoeben, W.F.L.M., et al., *On the Possibilities of Straightforward Characterization of Plasma Activated Water.* Plasma Chemistry and Plasma Processing, 2019. **39**(3): p. 597-626.
9. Punith, N., et al., *Plasma Activated Water Generation and its Application in Agriculture.* Advanced Materials Letters, 2019. **10**(10): p. 700-704.
10. Rathore, V. and S.K. Nema, *Optimization of process parameters to generate plasma activated water and study of physicochemical properties of plasma activated solutions at optimum condition.* Journal of Applied Physics, 2021. **129**(8).
11. Soni, A., J. Choi, and G. Brightwell, *Plasma-Activated Water (PAW) as a Disinfection Technology for Bacterial Inactivation with a Focus on Fruit and Vegetables.* Foods, 2021. **10**(1).
12. Li, Y., et al., *In vitro studies of the antimicrobial effect of non-thermal plasma-activated water as a novel mouthwash.* Eur J Oral Sci, 2017. **125**(6): p. 463-470.
13. Guo, L., et al., *Plasma-activated water: An alternative disinfectant for S protein inactivation to prevent SARS-CoV-2 infection.* Chem Eng J, 2021. **421**: p. 127742.
14. Zhao, Y.M., et al., *Plasma-activated water: Physicochemical properties, microbial inactivation mechanisms, factors influencing antimicrobial effectiveness, and applications in the food industry.* Compr Rev Food Sci Food Saf, 2020. **19**(6): p. 3951-3979.
15. Rifna, E.J., K. Ratish Ramanan, and R. Mahendran, *Emerging technology applications for improving seed germination.* Trends in Food Science & Technology, 2019. **86**: p. 95-108.
16. Li, Y., et al., *Evaluation of Cold Plasma Treatment and Safety in Disinfecting 3-week Root Canal Enterococcus faecalis Biofilm In Vitro.* J Endod, 2015. **41**(8): p. 1325-30.
17. Kim, S. and C.H. Kim, *Applications of Plasma-Activated Liquid in the Medical Field.* Biomedicines, 2021. **9**(11).
18. Ali, M., J.H. Cheng, and D.W. Sun, *Effect of plasma activated water and buffer solution on fungicide degradation from tomato (Solanum lycopersicum) fruit.* Food Chem, 2021. **350**: p. 129195.
19. Lukes, P., et al., *Aqueous-phase chemistry and bactericidal effects from an air discharge plasma in contact with water: evidence for the formation of peroxynitrite through a pseudo-second-order post-discharge reaction of H2O2and HNO2.* Plasma Sources Science and Technology, 2014. **23**(1): p. 015019.
20. Boopathy, B., et al., *Generation of Species-Specific High-Strength Plasma Activated Water at Neutral pH and its Antimicrobial Characteristics.* Plasma Chemistry and Plasma Processing, 2024. **44**(2): p. 1003-1017.
21. N., P., et al., *Generation of neutral pH high-strength plasma-activated water from a pin to water discharge and its bactericidal activity on multidrug-resistant pathogens.* Plasma Processes and Polymers, 2023. **20**(1): p. 2200133.
22. Morris, F.C., et al., *The Mechanisms of Disease Caused by Acinetobacter baumannii.* Front Microbiol, 2019. **10**: p. 1601.
23. Qin, S., et al., *Pseudomonas aeruginosa: pathogenesis, virulence factors, antibiotic resistance, interaction with host, technology advances and emerging therapeutics.* Signal Transduct Target Ther, 2022. **7**(1): p. 199.
24. Roy Chowdhury, A., et al., *Salmonella Typhimurium outer membrane protein A (OmpA) renders protection from nitrosative stress of macrophages by maintaining the stability of bacterial outer membrane.* PLoS Pathog, 2022. **18**(8): p. e1010708.
25. Hajra, D., et al., *Salmonella Typhimurium U32 peptidase, YdcP, promotes bacterial survival by conferring protection against in vitro and in vivo oxidative stress.* Microb Pathog, 2022. **173**(Pt B): p. 105862.

26. Heaselgrave, W., P.W. Andrew, and S. Kilvington, *Acidified nitrite enhances hydrogen peroxide disinfection of Acanthamoeba, bacteria and fungi.* J Antimicrob Chemother, 2010. **65**(6): p. 1207-14.
27. Weller, R., et al., *Antimicrobial effect of acidified nitrite on dermatophyte fungi, Candida and bacterial skin pathogens.* J Appl Microbiol, 2001. **90**(4): p. 648-52.
28. Subramanian, P.S.G., et al., *Plasma-activated water from a dielectric barrier discharge plasma source for the selective treatment of cancer cells.* Plasma Processes and Polymers, 2020. **17**(8): p. 1900260.
29. Ju, S., et al., *Plasma-activated water for inactivation of Fusarium graminearum spores: An in-vitro wheat study.* LWT, 2023. **183**: p. 114815.
30. Beck, P. and R. Huber, *Detection of cell viability in cultures of hyperthermophiles.* FEMS Microbiology Letters, 1997. **148**(1): p. 11-14.
31. Goldstein, S. and G. Merenyi, *The chemistry of peroxynitrite: implications for biological activity.* Methods Enzymol, 2008. **436**: p. 49-61.
32. Ischiropoulos, H., *Biological tyrosine nitration: a pathophysiological function of nitric oxide and reactive oxygen species.* Arch Biochem Biophys, 1998. **356**(1): p. 1-11.
33. Liaudet, L., F.G. Soriano, and C. Szabo, *Biology of nitric oxide signaling.* Crit Care Med, 2000. **28**(4 Suppl): p. N37-52.
34. Gunaydin, H. and K.N. Houk, *Mechanisms of peroxynitrite-mediated nitration of tyrosine.* Chem Res Toxicol, 2009. **22**(5): p. 894-8.
35. Prolo, C., M.N. Alvarez, and R. Radi, *Peroxynitrite, a potent macrophage-derived oxidizing cytotoxin to combat invading pathogens.* Biofactors, 2014. **40**(2): p. 215-25.
36. Ko, W.C. and G.G. Stone, *In vitro activity of ceftazidime-avibactam and comparators against Gram-negative bacterial isolates collected in the Asia-Pacific region as part of the INFORM program (2015-2017).* Ann Clin Microbiol Antimicrob, 2020. **19**(1): p. 14.
37. Bulik, C.C., et al., *Comparison of meropenem MICs and susceptibilities for carbapenemase-producing Klebsiella pneumoniae isolates by various testing methods.* J Clin Microbiol, 2010. **48**(7): p. 2402-6.
38. Chowdhury, A.R., et al., *Loss of outer membrane protein A (OmpA) impairs the survival of Salmonella Typhimurium by inducing membrane damage in the presence of ceftazidime and meropenem.* J Antimicrob Chemother, 2022. **77**(12): p. 3376-3389.
39. Sheng, W.H., et al., *Identification of distinct ciprofloxacin susceptibility in Acinetobacter spp. by detection of the gyrA gene mutation using real-time PCR.* Mol Cell Probes, 2009. **23**(3-4): p. 154-6.
40. Chang, M.X., et al., *Contribution of Different Mechanisms to Ciprofloxacin Resistance in Salmonella spp.* Front Microbiol, 2021. **12**: p. 663731.
41. O'Leary, K., *Reducing surgical site infections in low-resource settings.* Nat Med, 2022.
42. Surgery, N.G.R.H.U.o.G., *Reducing surgical site infections in low-income and middle-income countries (FALCON): a pragmatic, multicentre, stratified, randomised controlled trial.* Lancet, 2021. **398**(10312): p. 1687-1699.
43. McLean, K.A., et al., *Remote diagnosis of surgical-site infection using a mobile digital intervention: a randomised controlled trial in emergency surgery patients.* NPJ Digit Med, 2021. **4**(1): p. 160.
44. Serra, R., et al., *Altered metalloproteinase-9 expression as least common denominator between varicocele, inguinal hernia, and chronic venous disorders.* Ann Vasc Surg, 2014. **28**(3): p. 705-9.
45. Amato, B., et al., *Role of matrix metalloproteinases in non-healing venous ulcers.* Int Wound J, 2015. **12**(6): p. 641-5.
46. Renner, R., et al., *Persistence of bacteria like Pseudomonas aeruginosa in non-healing venous ulcers.* Eur J Dermatol, 2012. **22**(6): p. 751-7.

47. Serra, R., et al., *Chronic wound infections: the role of Pseudomonas aeruginosa and Staphylococcus aureus.* Expert Rev Anti Infect Ther, 2015. **13**(5): p. 605-13.
48. Cabral, B.G., et al., *Surgical Site Infection Following Caesarean Section by Acinetobacter Species: A Report from a Hyperendemic Setting in the Brazilian Amazon Region.* Microorganisms, 2021. **9**(4).
49. Llor, C. and L. Bjerrum, *Antimicrobial resistance: risk associated with antibiotic overuse and initiatives to reduce the problem.* Ther Adv Drug Saf, 2014. **5**(6): p. 229-41.
50. Tripathy, A., et al., *A Nanowire-Based Flexible Antibacterial Surface Reduces the Viability of Drug-Resistant Nosocomial Pathogens.* ACS Applied Nano Materials, 2018. **1**(6): p. 2678-2688.
51. Mai-Prochnow, A., et al., *Interactions of plasma-activated water with biofilms: inactivation, dispersal effects and mechanisms of action.* NPJ Biofilms Microbiomes, 2021. **7**(1): p. 11.
52. Charoux, C.M.G., et al., *Antimicrobial effects of airborne acoustic ultrasound and plasma activated water from cold and thermal plasma systems on biofilms.* Sci Rep, 2020. **10**(1): p. 17297.
53. Mizoi, K., et al., *Interactions between pH, reactive species, and cells in plasma-activated water can remove algae.* RSC Adv, 2022. **12**(13): p. 7626-7634.
54. Radi, R., *Peroxynitrite, a stealthy biological oxidant.* J Biol Chem, 2013. **288**(37): p. 26464-72.
55. Judee, F., et al., *Plasma-activation of tap water using DBD for agronomy applications: Identification and quantification of long lifetime chemical species and production/consumption mechanisms.* Water Res, 2018. **133**: p. 47-59.
56. Adhikari, B., et al., *Cold Atmospheric Plasma-Activated Water Irrigation Induces Defense Hormone and Gene expression in Tomato seedlings.* Scientific Reports, 2019. **9**(1).
57. Pang, B., et al., *Investigation of the chemical characteristics and anticancer effect of plasma-activated water: The effect of liquid temperature.* Plasma Processes and Polymers, 2022. **19**(1): p. 2100079.
58. Mahdikia, H., B. Shokri, and A.K. Majidzadeh, *The Feasibility Study of Plasma-activated Water as a Physical Therapy to Induce Apoptosis in Melanoma Cancer Cells In-vitro.* Iran J Pharm Res, 2021. **20**(3): p. 337-350.
59. Chauvin, J., et al., *Analysis of reactive oxygen and nitrogen species generated in three liquid media by low temperature helium plasma jet.* Sci Rep, 2017. **7**(1): p. 4562.
60. Girard, F., et al., *Formation of reactive nitrogen species including peroxynitrite in physiological buffer exposed to cold atmospheric plasma.* RSC Advances, 2016. **6**(82): p. 78457-78467.
61. Stokes, J.M., et al., *Bacterial Metabolism and Antibiotic Efficacy.* Cell Metab, 2019. **30**(2): p. 251-259.
62. Girotti, A.W., *Photodynamic lipid peroxidation in biological systems.* Photochemistry and photobiology, 1990. **51**(4): p. 497-509.
63. Al-Sharify, Z.T., T.A. Al-Sharify, and A.M. al-Azawi. *Investigative study on the interaction and applications of plasma activated water (PAW)*. in *IOP Conference Series: Materials Science and Engineering*. 2020. IOP Publishing.
64. Li, Y., et al., *In vitro studies of the antimicrobial effect of non-thermal plasma-activated water as a novel mouthwash.* European journal of oral sciences, 2017. **125**(6): p. 463-470.
65. Su, X., et al., *The role of high voltage electrode material in the inactivation of E. coli by direct-in-liquid electrical discharge plasma.* Plasma Chemistry and Plasma Processing, 2019. **39**: p. 577-596.
66. Xiang, Q., et al., *Antibacterial activity and a membrane damage mechanism of plasma-activated water against Pseudomonas deceptionensis CM2.* Lwt, 2018. **96**: p. 395-401.
67. Zhang, Q., et al., *A study of oxidative stress induced by non-thermal plasma-activated water for bacterial damage.* Applied physics letters, 2013. **102**(20).
68. Jyung, S., J.-W. Kang, and D.-H. Kang, *L. monocytogens exhibited less cell membrane damage, lipid peroxidation, and intracellular reactive oxygen species accumulation after plasma-*

activated water treatment compared to E. coli O157:H7 and S. Typhimurium. Food Microbiology, 2022. **108**: p. 104098.
69. Ischiropoulos, H., *Protein tyrosine nitration—an update.* Archives of biochemistry and biophysics, 2009. **484**(2): p. 117-121.
70. Lee, J., J.A. Hunt, and J.T. Groves, *Manganese porphyrins as redox-coupled peroxynitrite reductases.* Journal of the American Chemical Society, 1998. **120**(24): p. 6053-6061.
71. Salgo, M., et al., *Peroxynitrite causes DNA damage and oxidation of thiols in rat thymocytes [corrected].* Archives of biochemistry and biophysics, 1995. **322**(2): p. 500-505.
72. Ferrer-Sueta, G. and R. Radi, *Chemical biology of peroxynitrite: kinetics, diffusion, and radicals.* ACS chemical biology, 2009. **4**(3): p. 161-177.
73. McLean, S., et al., *Peroxynitrite toxicity in Escherichia coli K12 elicits expression of oxidative stress responses and protein nitration and nitrosylation.* J Biol Chem, 2010. **285**(27): p. 20724-31.
74. Curry-McCoy, T.V., N.A. Osna, and T.M. Donohue Jr, *Modulation of lysozyme function and degradation after nitration with peroxynitrite.* Biochimica et Biophysica Acta (BBA)-General Subjects, 2009. **1790**(8): p. 778-786.
75. Kohr, M.J., J.P. Davis, and M.T. Ziolo, *Peroxynitrite increases protein phosphatase activity and promotes the interaction of phospholamban with protein phosphatase 2a in the myocardium.* Biophysical Journal, 2009. **96**(3): p. 514a-515a.
76. Vaishampayan, A. and E. Grohmann, *Antimicrobials Functioning through ROS-Mediated Mechanisms: Current Insights.* Microorganisms, 2021. **10**(1).
77. Kohanski, M.A., et al., *Bactericidal antibiotics promote reactive oxygen species formation and inflammation in human sinonasal epithelial cells.* Int Forum Allergy Rhinol, 2016. **6**(2): p. 191-200.
78. Kamali, E., et al., *In vitro activities of cellulase and ceftazidime, alone and in combination against Pseudomonas aeruginosa biofilms.* BMC Microbiol, 2021. **21**(1): p. 347.
79. Maleki, M.H., et al., *Detection of highly ciprofloxacin resistance acinetobacter baumannii isolated from patients with burn wound infections in presence and absence of efflux pump inhibitor.* Maedica (Bucur), 2014. **9**(2): p. 162-7.
80. Huo, W., et al., *Immunosuppression broadens evolutionary pathways to drug resistance and treatment failure during Acinetobacter baumannii pneumonia in mice.* Nat Microbiol, 2022. **7**(6): p. 796-809.
81. Ali Shah, S.A., et al., *Antimicrobial Sensitivity Pattern of Salmonella Typhi: Emergence of Resistant Strains.* Cureus, 2020. **12**(11): p. e11778.
82. Zhou, X. and P. He, *Improved measurements of intracellular nitric oxide in intact microvessels using 4,5-diaminofluorescein diacetate.* Am J Physiol Heart Circ Physiol, 2011. **301**(1): p. H108-14.
83. Myers, A.L., et al., *Inflammatory production of reactive oxygen species by Drosophila hemocytes activates cellular immune defenses.* Biochem Biophys Res Commun, 2018. **505**(3): p. 726-732.
84. Walch, M., et al., *Cytotoxic cells kill intracellular bacteria through granulysin-mediated delivery of granzymes.* Cell, 2014. **157**(6): p. 1309-1323.

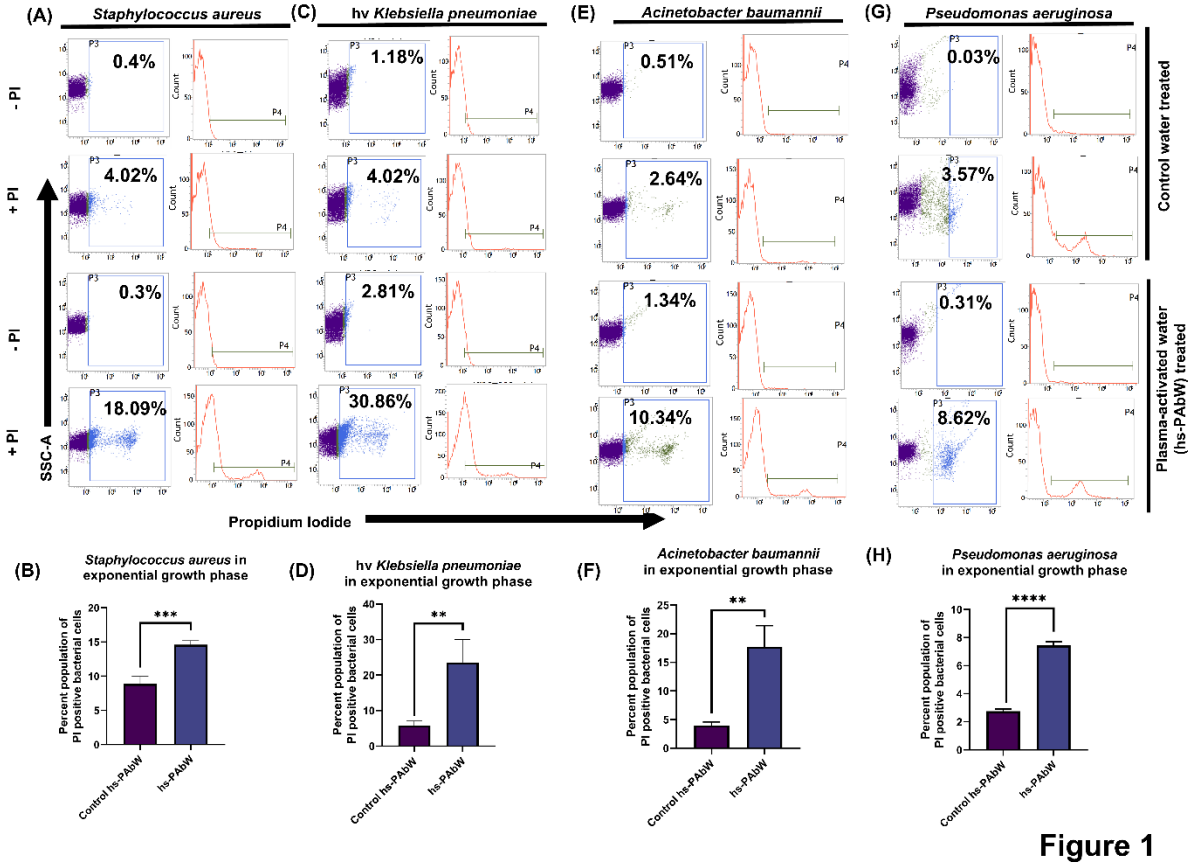

Figure 1. hs-PAbW induces a considerable amount of killing in exponentially growing bacteria.

(A, C, E and G) The dot plot (SSC-A vs. PI) and histogram (count vs. PI) represent the viability of exponentially growing cultures of *Staphylococcus* (A), hv *Klebsiella* (C), *Acinetobacter baumannii* (E), and *Pseudomonas aeruginosa* (E) with hs-PAbW. The bar graphs represent the propidium iodide positive percent population of *Staphylococcus* (B), hv *Klebsiella* (D), *Acinetobacter baumannii* (F), and *Pseudomonas aeruginosa* (H) with or without hs-PAbW treatment. The data are represented as mean ± SEM. (n≥3, N≥2).

(P)* *< 0.05, *(P)* **< 0.005, *(P)* ***< 0.0005, *(P)* *< 0.0001, ns= non-significant, (Unpaired two-tailed student's t-test).**

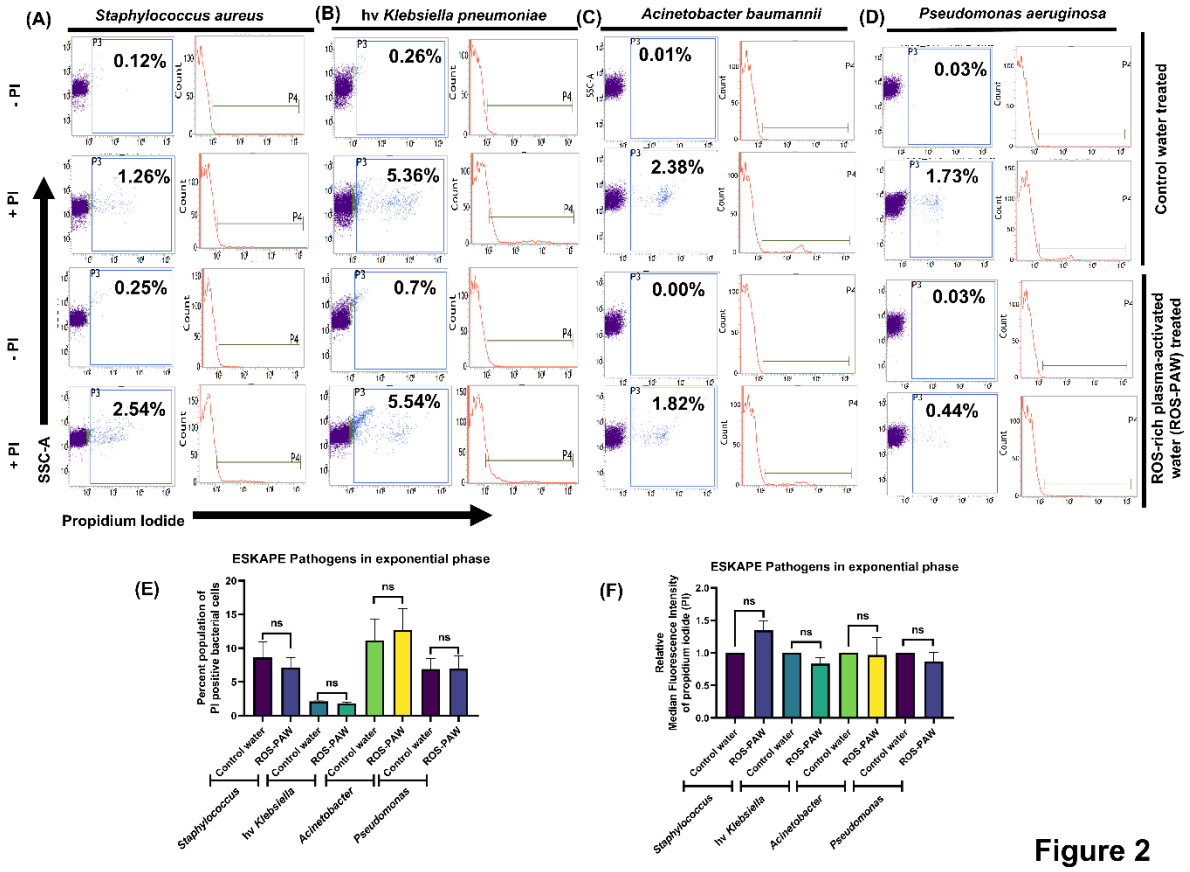

Figure 2. ROS-PAW itself is unable to induce bacterial death.

(A, B, C, and D) The dot plot (SSC-A vs. PI) and histogram (count vs. PI) represent the viability of exponentially growing *Staphylococcus* (A), hv *Klebsiella* (B), *Acinetobacter baumannii* (C), and *Pseudomonas aeruginosa* (D) treated with reactive oxygen species rich plasma-activated water (ROS-PAW). (D) The bar graphs represent the PI-positive percent population of *Staphylococcus*, hv *Klebsiella*, *Acinetobacter baumannii*, and *Pseudomonas aeruginosa* with or without ROS-PAW treatment. (E) The median fluorescence intensity (MFI) of the PI-positive population of *Staphylococcus*, hv *Klebsiella*, *Acinetobacter baumannii*, and *Pseudomonas aeruginosa* with or without ROS-PAW treatment (F). The data are represented as mean ± SEM. (n≥3, N=3).

(P)* *< 0.05, *(P)* **< 0.005, *(P)* ***< 0.0005, *(P)* *< 0.0001, ns= non-significant, (Unpaired two-tailed student's t-test).**

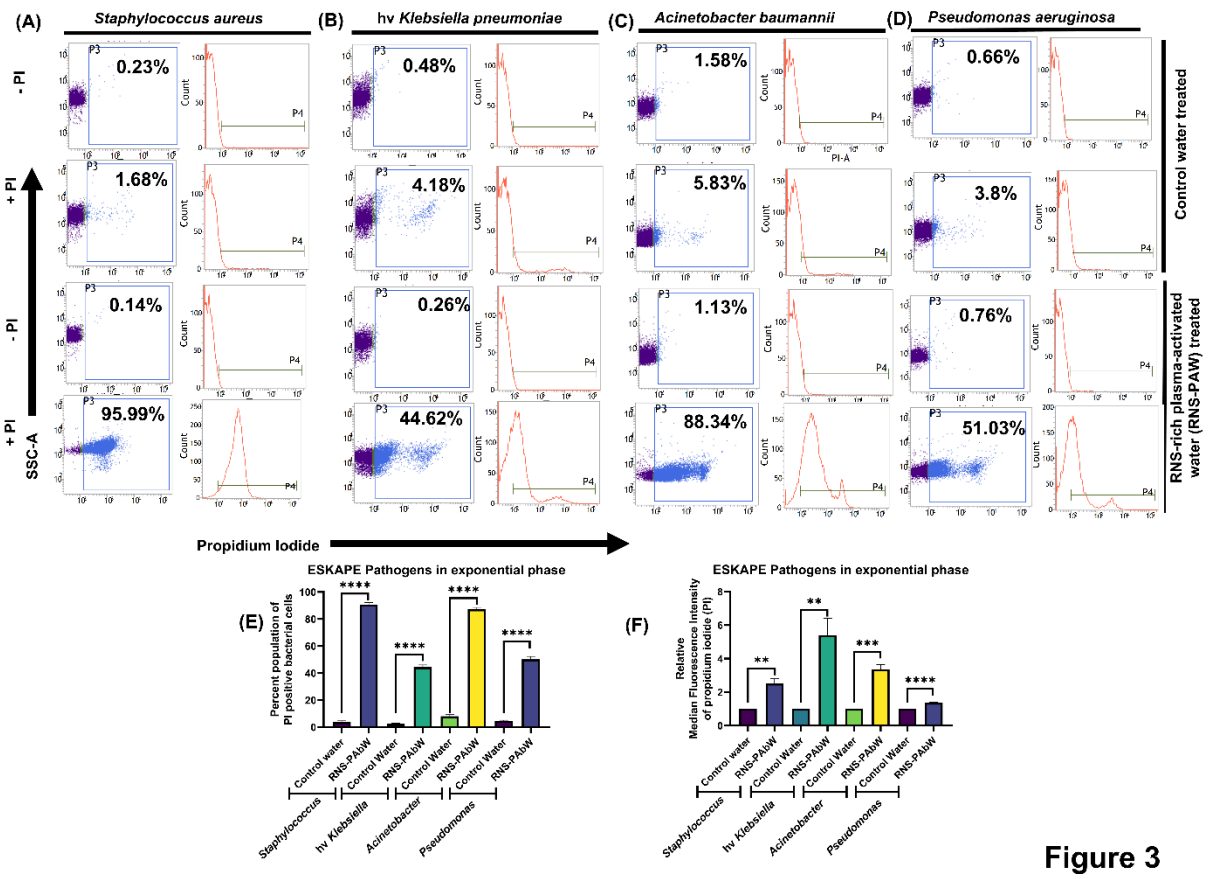

Figure 3. RNS-PAbW can kill exponentially growing bacteria independently.

(A, B, C, and D) The dot plot (SSC-A vs. PI) and histogram (count vs. PI) represent the viability of exponentially growing *Staphylococcus* (A), hv *Klebsiella* (B), *Acinetobacter baumannii* (C), and *Pseudomonas aeruginosa* (D) treated with reactive nitrogen species rich plasma-activated water (RNS-PAbW). The bar graphs represent the PI-positive percent population of *Staphylococcus*, hv *Klebsiella*, *Acinetobacter baumannii*, and *Pseudomonas aeruginosa* with or without RNS-PAbW treatment. (E) The relative median fluorescence intensity (MFI) of the PI-positive population of *Staphylococcus*, hv *Klebsiella*, *Acinetobacter baumannii*, and *Pseudomonas aeruginosa* with or without RNS-PAbW treatment (F). The data are represented as mean ± SEM. (n≥3, N=3).

(P)* *< 0.05, *(P)* **< 0.005, *(P)* ***< 0.0005, *(P)* *< 0.0001, ns= non-significant, (Unpaired two-tailed student's t-test).**

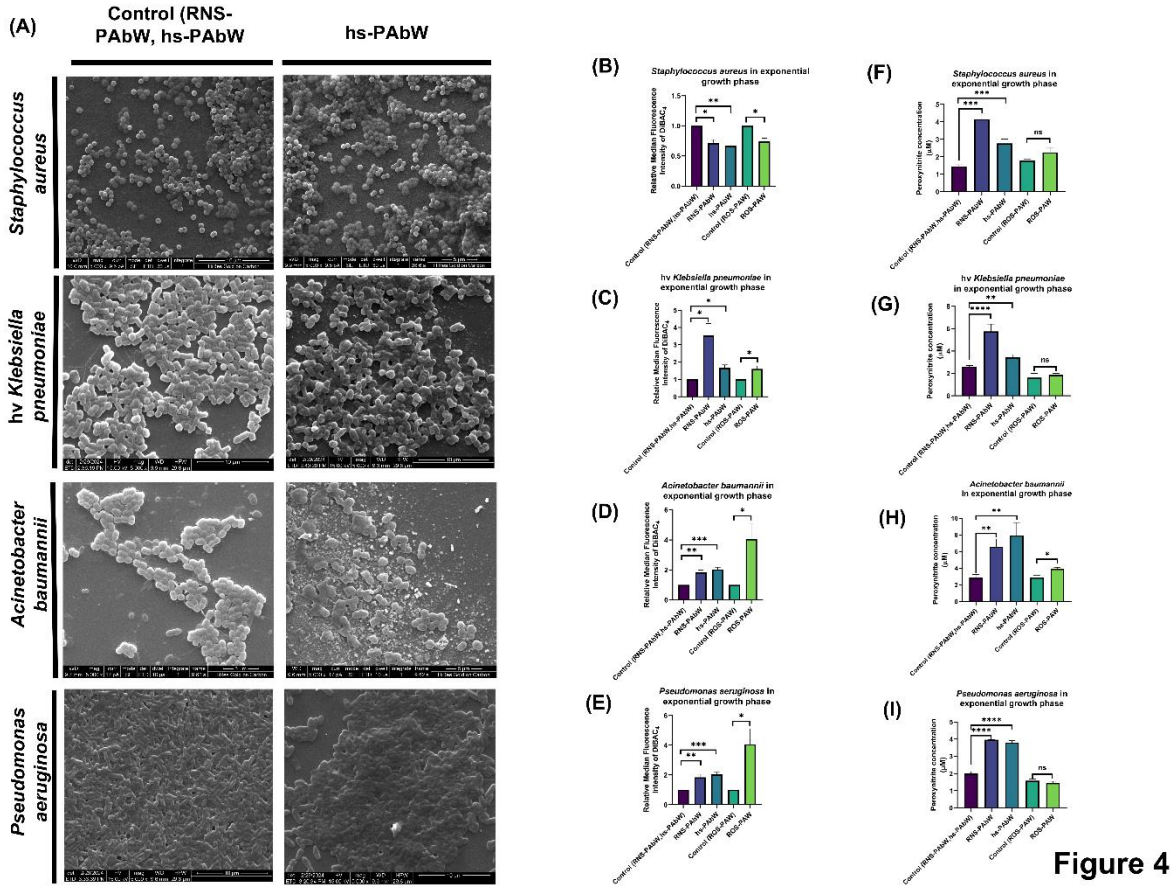

Figure 4. ROS-PAW can alter membrane potential, however, it is not sufficient for a bactericidal effect.

Scanning Electron Microscopy images of *Staphylococcus*, hv *Klebsiella*, *Acinetobacter*, *Pseudomonas* treated with hs-PAbW and control water (A). The relative median fluorescence intensity (MFI) of the $DiBAC_4$-positive population of *Staphylococcus*, hv *Klebsiella*, *Acinetobacter baumannii*, and *Pseudomonas aeruginosa* with RNS-PAbW, hs-PAbW, ROS-PAW treatment. is represented in figure panels B-E. The data are represented as mean ± SEM. ($n \geq 3$, N=3). Figure panels **F-I** contain the bar graphs that represent the quantity of intracellular peroxynitrite produced upon treatment with control ROS-PAW, ROS-PAW, control RNS-PAbW, RNS-PAbW, control hs-PAbW and hs-PAbW of *Staphylococcus* (B), hv *Klebsiella* (C), *Acinetobacter* (D), *Pseudomonas* (E). The data are represented as mean ± SD. ($n \geq 3$).

(P)* *< 0.05, *(P)* **< 0.005, *(P)* ***< 0.0005, *(P)* *< 0.0001, ns= non-significant, (Unpaired two-tailed student's t-test).**

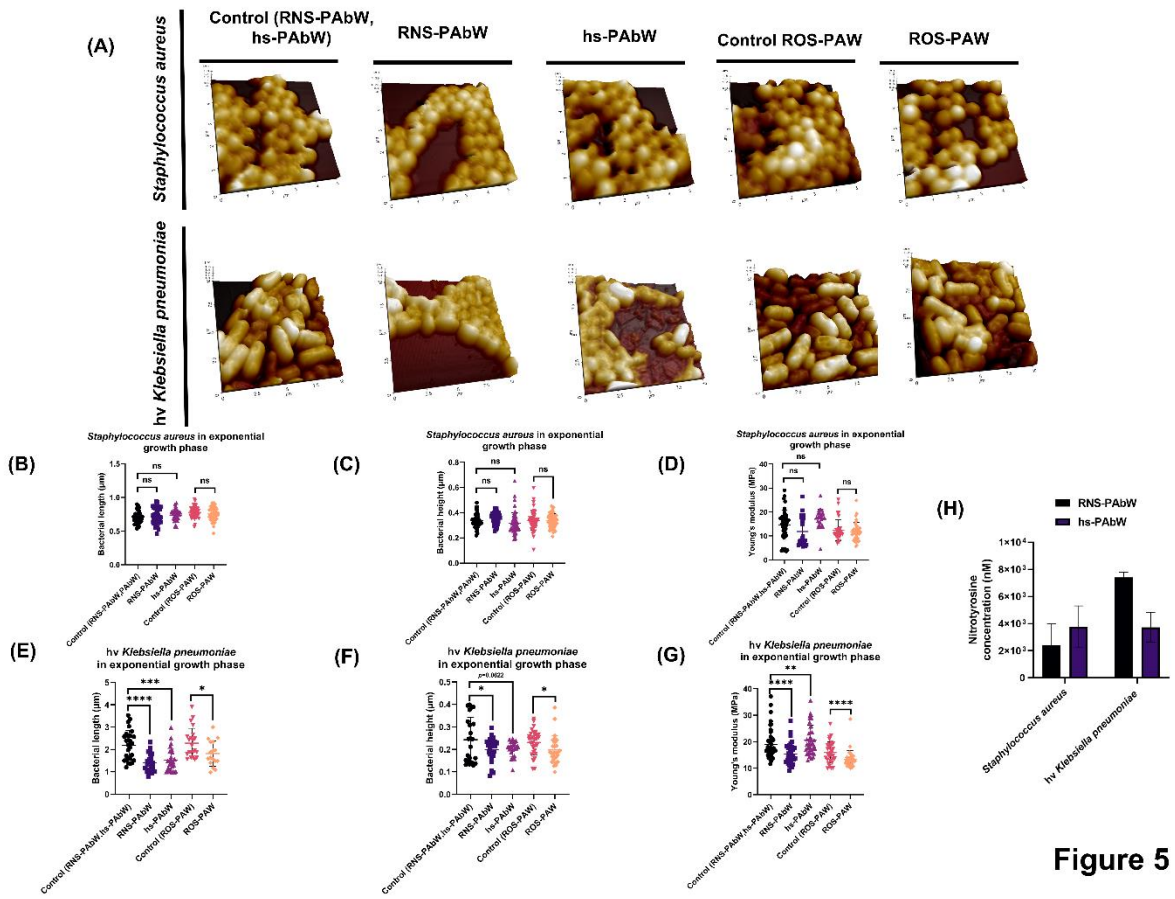

Figure 5. Treatment with RNS-PAbW, hs-PAbW, and ROS-PAbW resulted in a decrease in the length, height, and Young's modulus of the Gram-negative bacterium hv *Klebsiella pneumoniae* but had no such effect on the Gram-positive *Staphylococcus aureus*. Furthermore, RNS-PAbW and hs-PAbW treatments were associated with elevated nitrotyrosine levels, which were not observed in ROS-PAW or control water-treated cell lysates.

(A) Atomic Force Microscopy images of *Staphylococcus aureus* and hv *Klebsiella pneumoniae* after treatment with control waters, ROS-PAW, hs-PAbW, and RNS-PAbW. Quantification of the length, height, and Young's modulus for *Staphylococcus* (B, C, D) and *Klebsiella* (E, F, G) was performed. Data for (A-G) are representative data of N=2, n≥20, and are shown as mean±SD.

(H) shows intracellular nitrotyrosine levels in *Staphylococcus* and *Klebsiella* following treatment with RNS-PAbW and hs-PAbW. The data is a representative of N=2, n=3, and is presented as mean±SD.

(P)* *< 0.05, *(P)* **< 0.005, *(P)* ***< 0.0005, *(P)* *< 0.0001, ns= non-significant, (Unpaired two-tailed student's t-test).**

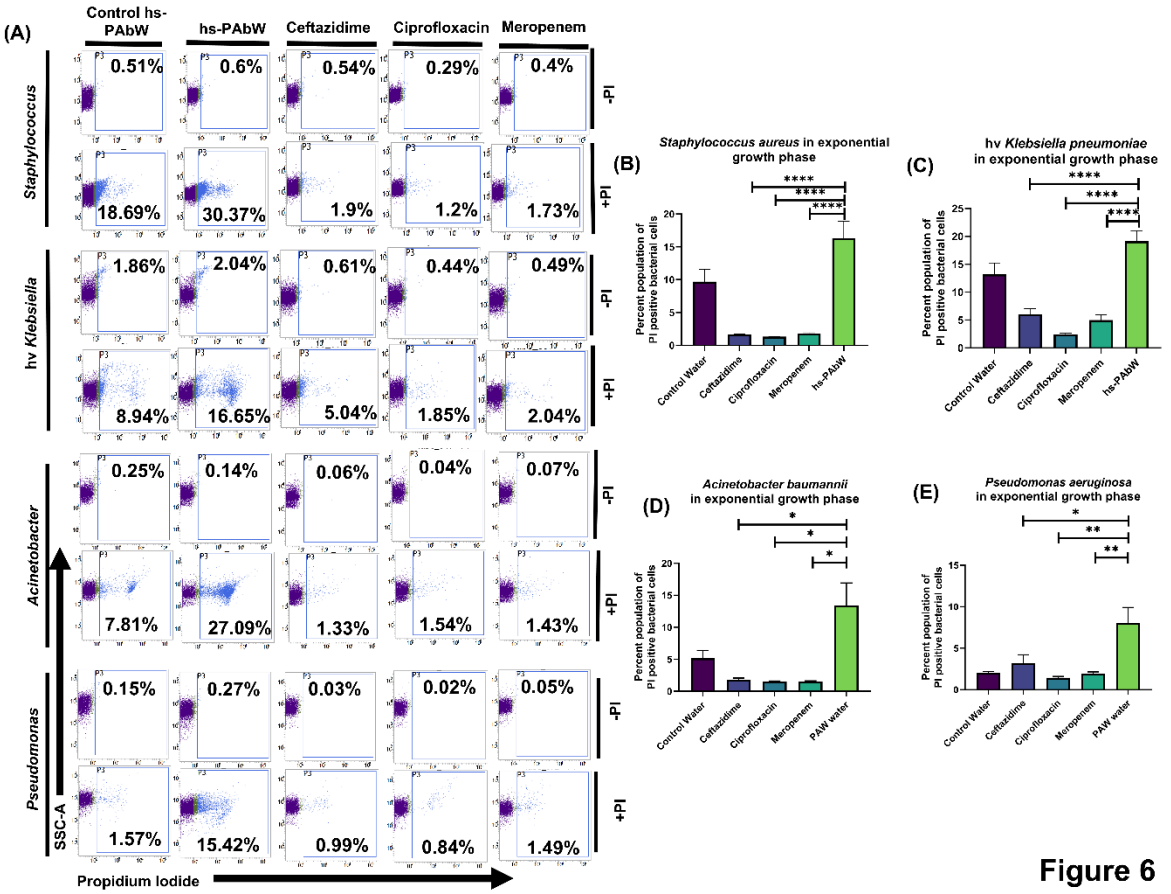

Figure 6. hs-PAbW induces bacterial death faster than high concentrations of antibiotics.

The dot plot (SSC-A vs. PI) and histogram (count vs. PI) represent the viability of exponentially growing *Staphylococcus*, hv *Klebsiella*, *Acinetobacter baumannii*, and *Pseudomonas aeruginosa*, treated with plasma-activated water (hs-PAbW) and 50µg/ mL concentrations of ceftazidime, ciprofloxacin, and meropenem (A). The bar graphs represent the PI-positive percent population of *Staphylococcus* (B), *hv Klebsiella* (C), *Acinetobacter baumannii* (D), and *Pseudomonas aeruginosa* (E) with or without hs-PAbW, ceftazidime, ciprofloxacin, and meropenem treatment. The data are represented as mean ± SEM. (n≥3, N=2).

(P)* *< 0.05, *(P)* **< 0.005, *(P)* ***< 0.0005, *(P)* *< 0.0001, ns= non-significant, (Unpaired two-tailed student's t-test).**

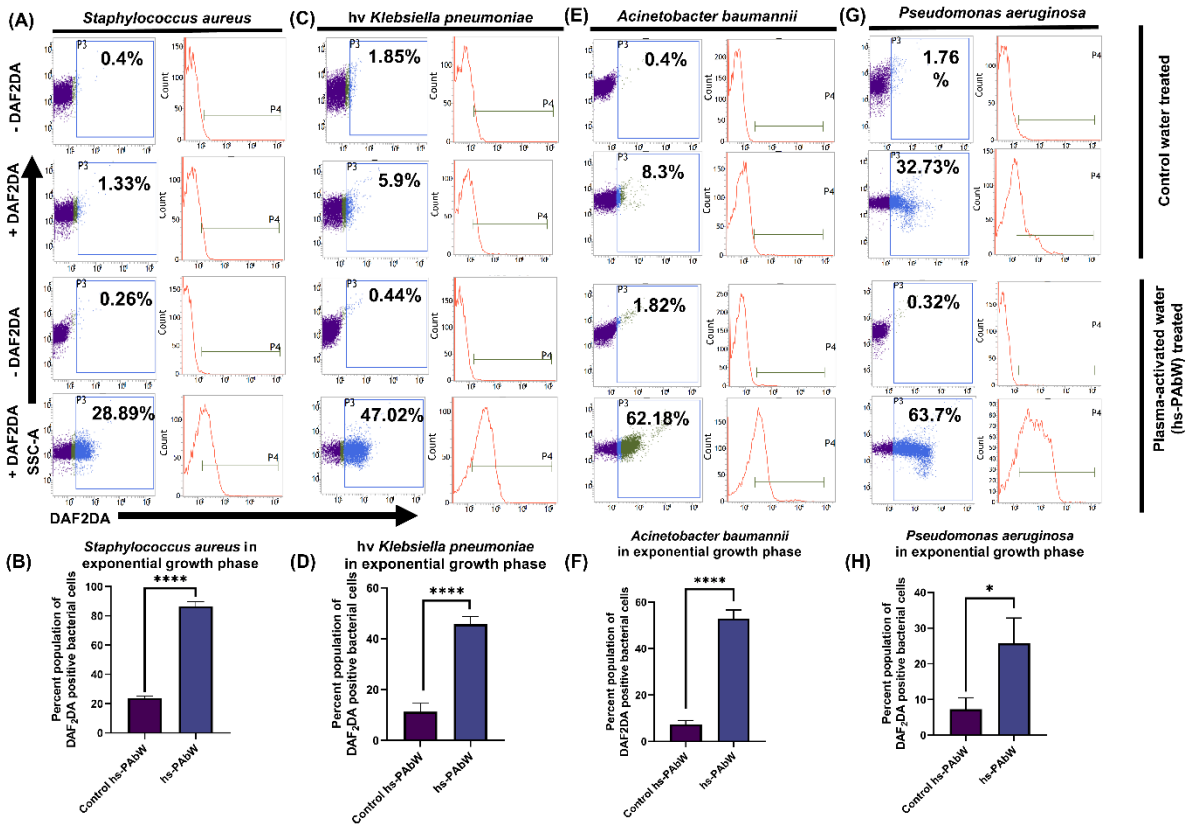

Figure S1. hs-PAbW-dependent generation of reactive nitrogen species while incubated with log-phase bacteria.

(A, C, E and G) The dot plot (SSC-A vs. DAF_2DA) and histogram (count vs. DAF_2DA) represent the generation of reactive nitrogen intermediates upon treating the exponentially growing cultures of *Staphylococcus* (A), hv *Klebsiella* (C), *Acinetobacter baumannii* (E), and *Pseudomonas aeruginosa* (E) with hs-PAbW. The bar graphs represent the DAF_2DA-positive percent population of *Staphylococcus* (B), hv *Klebsiella* (D), *Acinetobacter baumannii* (F), and *Pseudomonas aeruginosa* (H) with or without hs-PAbW treatment. The data are represented as mean ± SEM. ($n \geq 3$, $N \geq 2$).

(P)* *< 0.05, *(P)* **< 0.005, *(P)* ***< 0.0005, *(P)* *< 0.0001, ns= non-significant, (Unpaired two-tailed student's t-test).**

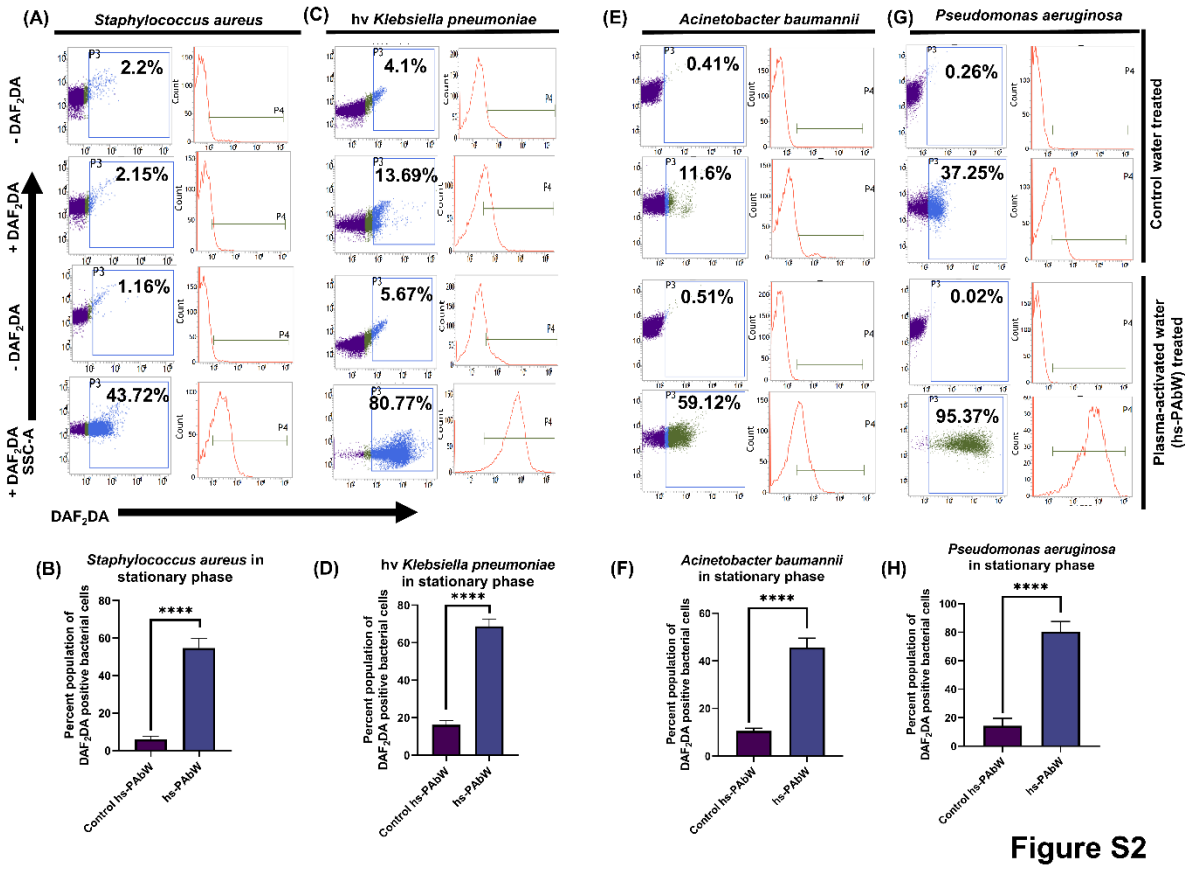

Figure S2. hs-PAbW-dependent generation of reactive nitrogen species while incubated with the stationary phase.

(A, C, E and G) The dot plot (SSC-A vs. DAF_2DA) and histogram (count vs. DAF_2DA) represent the generation of reactive nitrogen intermediates upon treating the stationary phase cultures of *Staphylococcus* (A), hv *Klebsiella* (C), *Acinetobacter baumannii* (E), and *Pseudomonas aeruginosa* (E) with hs-PAbW. The bar graphs represent the DAF_2DA-positive percent population of *Staphylococcus* (B), hv Klebsiella (D), *Acinetobacter baumannii* (F), and *Pseudomonas aeruginosa* (H) with or without hs-PAbW treatment. The data are represented as mean ± SEM. (n≥3, N≥2).

(P)* *< 0.05, *(P)* **< 0.005, *(P)* ***< 0.0005, *(P)* *< 0.0001, ns= non-significant, (Unpaired two-tailed student's t-test).**

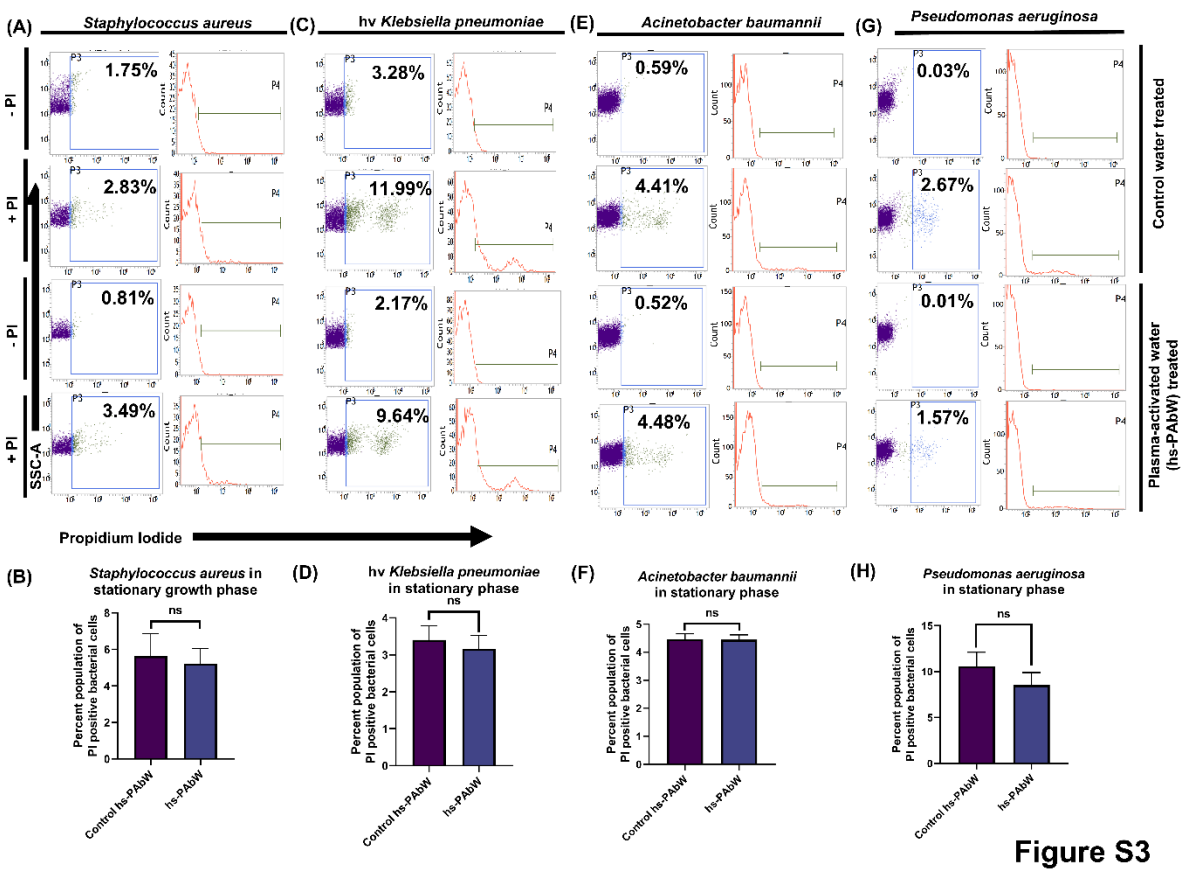

Figure S3. hs-PAbW couldn't kill the stationary phase cultures of bacteria.

(A, C, E and G) The dot plot (SSC-A vs. PI) and histogram (count vs. PI) represent the viability of exponentially growing cultures of *Staphylococcus* (A), hv *Klebsiella* (C), *Acinetobacter baumannii* (E), and *Pseudomonas aeruginosa* (E) with hs-PAbW. The bar graphs represent the propidium iodide positive percent population of *Staphylococcus* (B), hv *Klebsiella* (D), *Acinetobacter baumannii* (F), and *Pseudomonas aeruginosa* (H) with or without hs-PAbW treatment. The data are represented as mean ± SEM. (n≥3, N≥2).

(P)* *< 0.05, *(P)* **< 0.005, *(P)* ***< 0.0005, *(P)* *< 0.0001, ns= non-significant, (Unpaired two-tailed student's t-test).**

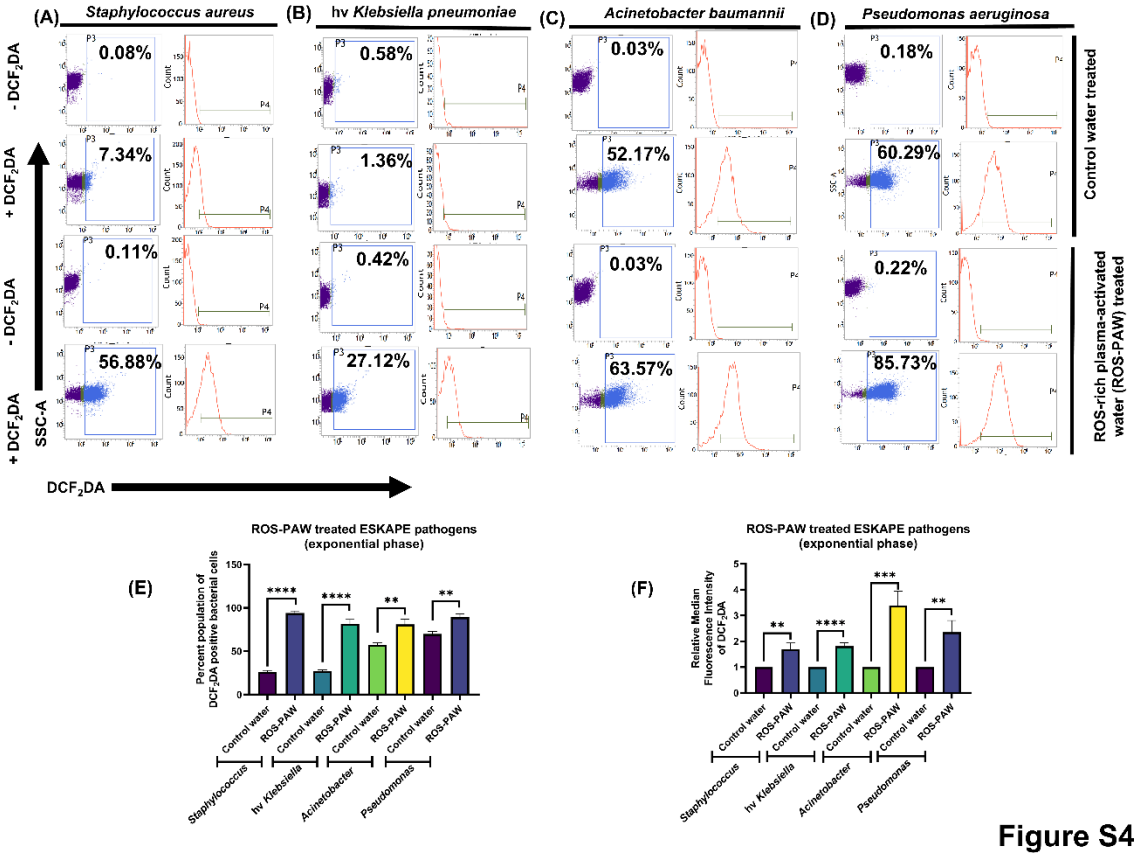

Figure S4. ROS-PAW generates a significant amount of ROS.

(A, B, C, and D) The dot plot (SSC-A vs. DCF_2DA) and histogram (count vs. DCF_2DA) represent the ROS content of exponentially growing *Staphylococcus* (A), hv *Klebsiella* (B), *Acinetobacter baumannii* (C), and *Pseudomonas aeruginosa* (D) treated with reactive oxygen species rich plasma-activated water (ROS-PAW). The bar graphs represent the DCF_2DA-positive percent population of *Staphylococcus*, hv *Klebsiella*, *Acinetobacter baumannii*, and *Pseudomonas aeruginosa* with or without ROS-PAW treatment (E). The relative median fluorescence intensity (MFI) of the DCF_2DA-positive population of *Staphylococcus*, hv *Klebsiella*, *Acinetobacter baumannii*, and *Pseudomonas aeruginosa* with or without ROS-PAW treatment (F). The data are represented as mean ± SEM. ($n \geq 3$, N=3).

(P)* *< 0.05, *(P)* **< 0.005, *(P)* ***< 0.0005, *(P)* *< 0.0001, ns= non-significant, (Unpaired two-tailed student's t-test).**

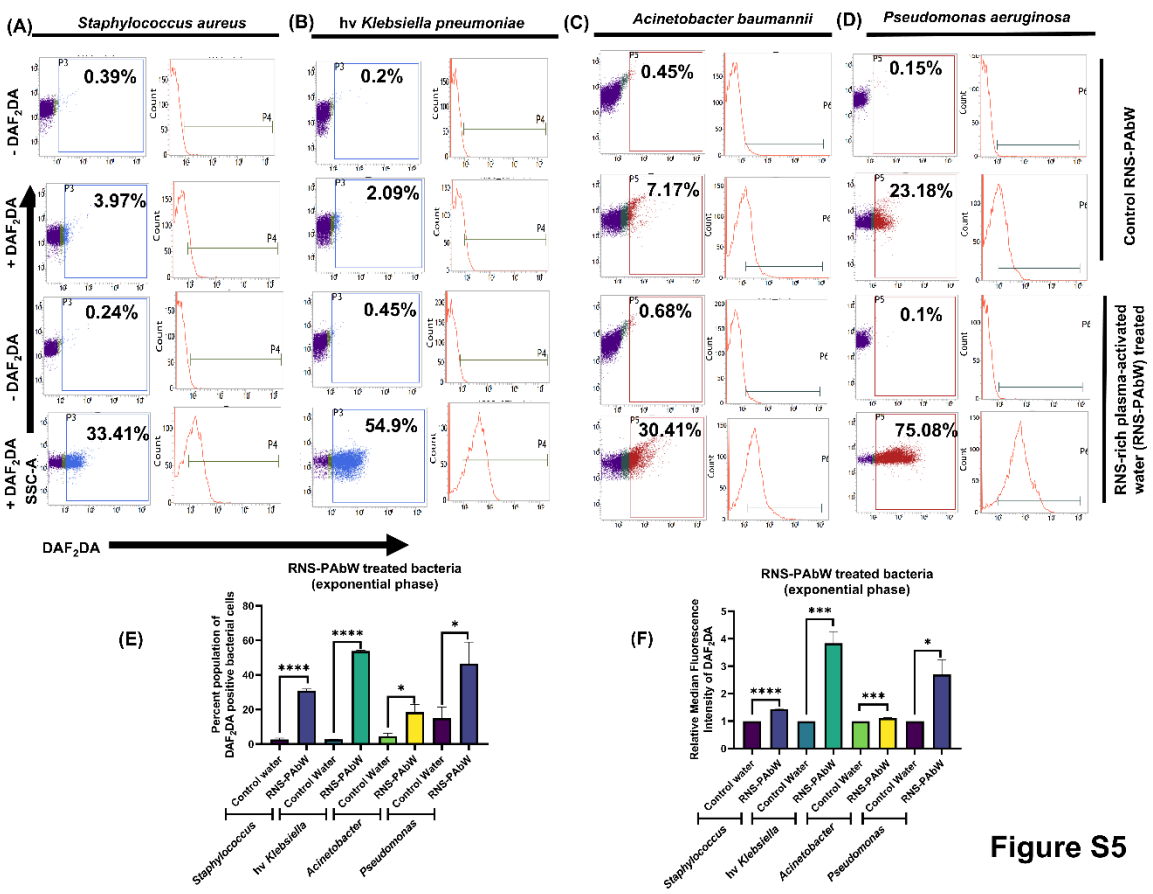

Figure S5. RNS-PAbW generates high amount of reactive nitrogen species in the treated bacteria.

(A, B, C, and D) The dot plot (SSC-A vs. DAF_2DA) and histogram (count vs. DAF_2DA) represent the RNS content of exponentially growing *Staphylococcus* (A), hv *Klebsiella* (B), *Acinetobacter baumannii* (C), and *Pseudomonas aeruginosa* (D) treated with reactive nitrogen species rich plasma-activated water (RNS-PAbW). The bar graphs represent the DAF_2DA-positive percent population of *Staphylococcus*, hv *Klebsiella*, *Acinetobacter baumannii*, and *Pseudomonas aeruginosa* with or without RNS-PAbW treatment (E). The median fluorescence intensity (MFI) of the DAF_2DA-positive population of *Staphylococcus*, hv *Klebsiella*, *Acinetobacter baumannii*, and *Pseudomonas aeruginosa* with or without RNS-PAbW treatment (F). The data are represented as mean ± SEM. ($n \geq 3$, N=3).

(P)* *< 0.05, *(P)* **< 0.005, *(P)* ***< 0.0005, *(P)* *< 0.0001, ns= non-significant, (Unpaired two-tailed student's t-test).**

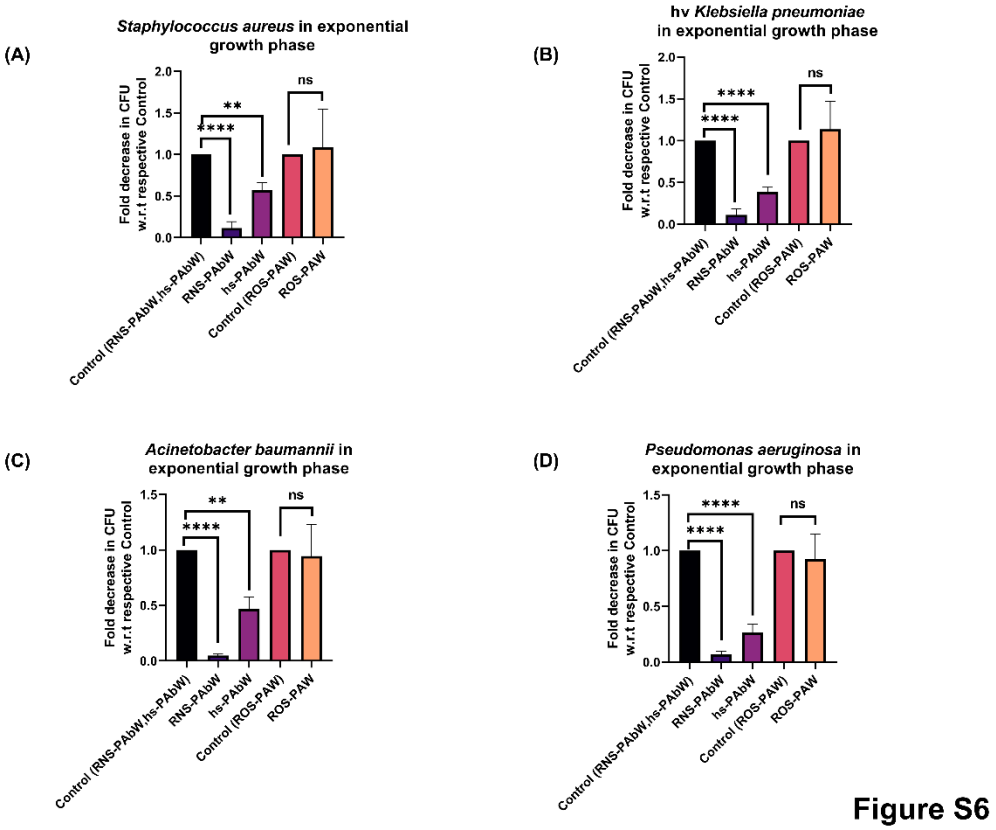

Figure S6. Incubation with RNS-PAbW and hs-PAbW results in significant reduction of Colony Forming Units, but not ROS-PAW

The column graphs represent the fold decrease in CFU after treatment with RNS-PAbW, hs-PAbW, and ROS-PAW compared to the respective control water samples for *Staphylococcus aureus* (A), hv *Klebsiella pneumoniae* (B), *Acinetobacter baumannii* (C), and *Pseudomonas aeruginosa* (D).

(P)* *< 0.05, *(P)* **< 0.005, *(P)* ***< 0.0005, *(P)* *< 0.0001, ns= non-significant, (Unpaired two-tailed student's t-test).**

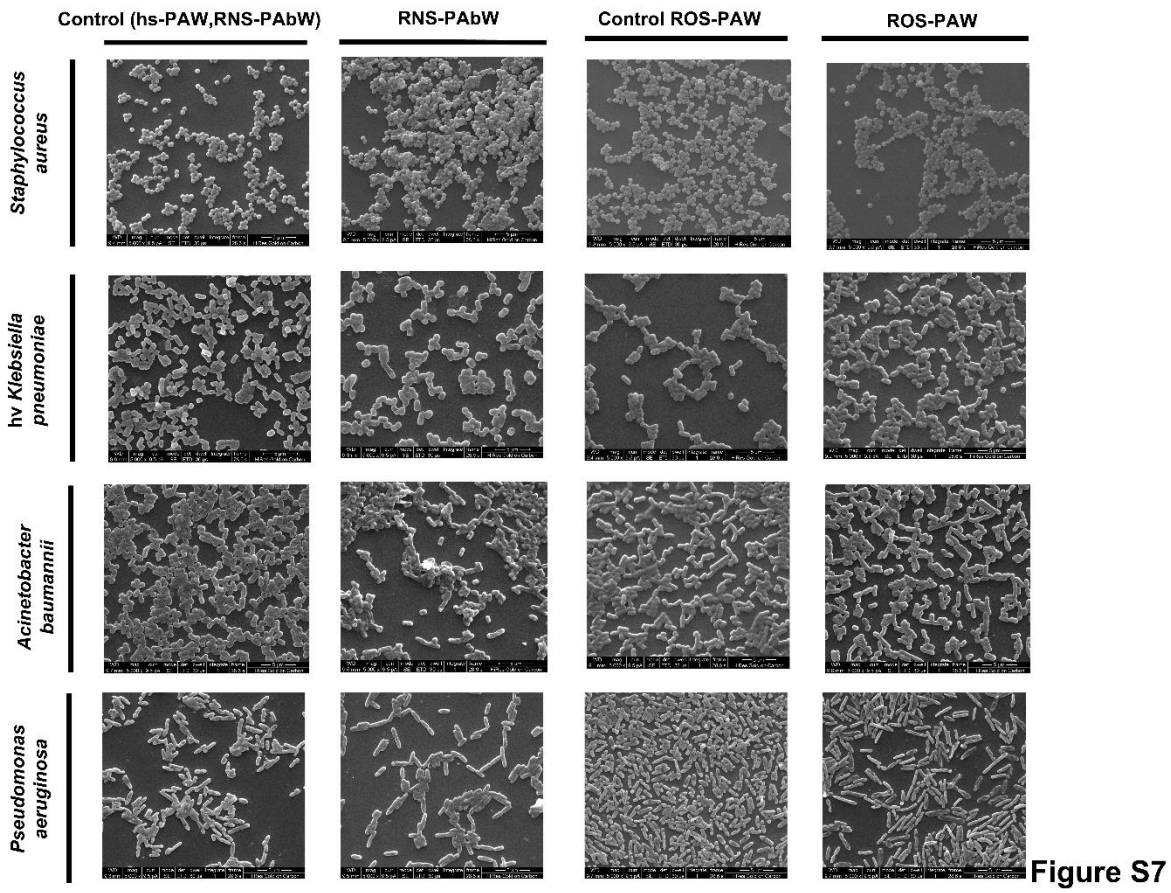

Figure S7. Scanning Electron Microscopy to study morphological change in the bacterial samples post exposure to RNS-PAbW and ROS-PAW

(A)

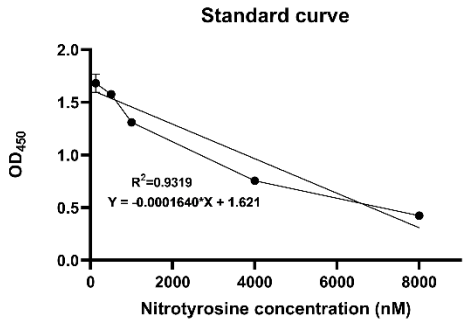

(B)

OD_{450}	OD_{450}	OD_{450}		
2.2022	2.1626	2.088	Control (RNS-PAbW, PAbW)	*Staphylococcus aureus*
1.0671	1.5135	1.3933	RNS-PAbW	
0.906	1.3581	1.1124	hs-PAbW	
3.5378	3.344	3.6628	Control ROS-PAW	
3.696	3.4822	3.6582	ROS-PAW	
2.059	2.0361	1.7912	Control (RNS-PAbW, PAbW)	hv *Klebsiella pneumoniae*
0.6262	0.5272	0.615	RNS-PAbW	
0.9492	1.2645	1.1758	hs-PAbW	
3.0252	3.0718	2.9592	Control ROS-PAW	
3.0177	3.0131	3.236	ROS-PAW	

Figure S8

Figure S8: Nitrotyrosine estimation reveals a significant increase in nitrotyrosine levels following treatment with RNS-PAbW and hs-PAbW, but not with ROS-PAW.

A standard curve (A) was generated using the OD_{450} absorbance values of the nitrotyrosine standards, and the nitrotyrosine concentration in the samples was determined by interpolating the raw data (B) against the standard curve.